Method of physical and enzymatic concentration of extraneous materials in wheat flour to enable near infrared chemical imaging

by

Tyler R. Nickoley

B.A., Kansas State University, 2011

A THESIS

submitted in partial fulfillment of the requirements for the degree

MASTER OF SCIENCE

Food Science

KANSAS STATE UNIVERSITY
Manhattan, Kansas

2018

Approved by:

_____

Major Professor
Dr. David L. Wetzel

Copyright

Abstract

Grain processing and handling requires quality determinations to ensure wholesome products that meet or surpass legal standards and specifications required by the end consumer. Near infrared spectroscopy has proven to be a useful and versatile tool to enable grain processers to make adjustments as needed. Near infrared chemical imaging also provides spatial information within the image and relative composition of chemically distinct components within the product. The potential use of chemical imaging to determine extraneous material in bread baking quality flour was addressed. A specimen preparation technique was developed. Insect fragment spiked specimens were imaged to determine their imaging effectiveness for application near the allowable limit of insect fragment concentration. Imaging was achieved using indium antimonide array detection of diffusely reflected radiation. The detector array of 81,920 pixels collected radiation from an area of 30.72 mm by 38.4 mm with a pixel size of 120 μm^2. Spectra were collected simultaneously from each pixel without moving parts by scanning with a liquid crystal tunable filter. Partial least squares analysis of each pixel within the sample allowed a summation of the insect quantity. The chemical structural distinction of chitin in the high protein matrix of the insect residue was in contrast to the non-digested carbohydrate residue in the lesser protein matrix of the flour. The method developed provided a linear response for a concentration range from approximately half the allowable limit to twice the limit for two insects that commonly contaminate flour. For the two insects studied the slopes are comparable with a slight off-set over a practical working range, so that insect concentration can be determined independently of species recognition.

Table of Contents

List of Figures

List of Tables

List of Abbreviations

LCTF – liquid crystal tunable filter

DAL – defect action level

FPA – focal plan array

PLS – partial least square

FOV – field of view

InGaAs – indium gallium arsenide

InSb – indium antimonide

ppt – parts per thousand

Acknowledgements

I would first like to acknowledge and thank Dr. Wetzel for working with me and teaching me about spectroscopy. He leads the Microbeam Molecular Spectroscopy laboratory, which houses the sophisticated near infrared imaging instrument. Mark Boatwright, another member of the laboratory, whose experience has been a great help, has given valuable time and effort on this project. Dr. Subramanyam, head of the Grain Science Entomology laboratory for providing live insect colonies and the knowledge to increase their numbers for testing. The Grain Science Department, allowed us to use a Rotap® sieve to complete the experiment. I would like to thank my committee members: Dr. Wetzel, Dr. Smith, and Dr. Seib for reading and strengthening the thesis.

Preface

The Sapphire® NIR chemical imaging system paired with the ISys® processing software of Spectral Dimensions Inc., (Olney, MD, USA) was used in this experiment. Dr. Linda Kidder and Dr. Neal Lewis designed the instrument and software and started Spectral Dimensions Inc. for the pharmaceutical industry to determine the uniformity and concentration of active components of medications in batch mixtures and tablets (Lewis et al., 2005). The cited article is titled *NIR Imaging- near infrared Spectroscopy on Steroids*; it highlights this instrument's ability to distinguish the difference of the core and the coating of one microsphere, and to count and distinguish the amount of a mixture of two chemically distinct microspheres. In an earlier study using a similar imaging instrument and processing software, pharmaceutical mixtures of furosemide were collected with varying mixing times, showing which mixing time was needed to insure the furosemide tablet would be uniform in the active component and cellulose filler (Lyon, 2002). Similar focal plan array (FPA) detectors consisting of multiple detector elements of indium antimonide (InSb) were used earlier in foray transform infrared spectroscopy to chemically image heterogeneous materials in biological and polymer material (Lewis et al., 1995).

The Microbeam Molecular Spectroscopy Laboratory at Kansas State University uses the Sapphire® instrument and the ISys® software, which was originally designed to distinguish pure chemicals, to image heterogeneous mixtures of organic solids to help optimize milling by reducing non-endosperm material in flour streams in a mill (Wetzel, 2013). In addition, in the feed industry, previous research (Wetzel et al., 2010) determined how much mixing is needed to blend proteins into a meal prior to extrusion processing. Another variation on the instrument's

use was to collect chemical information to search individual grain kernels for sprout damage to determine the germination rate for kernels used for planting (Smail et al., 2006).

Using the instrument to identify the amount of insect material in flour pushed the limits of the instrument even further. The low defect action level (DAL) set by the FDA, required a concentration step. The near infrared region was useful for quickly determining relative concentrations in many biological materials; however, it was not sensitive enough to find a trace amount of a component. This is especially true for biological components in a mixture instead of a pure chemical. A concentration step was finally found that could allow the instrument to distinguish and quantify the insect fragments in a sample.

Part 1 - Introduction

1.1 - Importance of insect fragment detection method

During the processing and storage of cereal products, there are many things that can reduce the purity and value of the commodity. Infestation of various insect species is a serious issue that can diminish the nutrient value of the cereal grain and ultimately decrease the end product yield and quality. Prior to milling, while the whole grain is being shipped, the whole kernel can be analyzed for insects by flotation or x-ray analysis to prevent infested grain from being processed. The milled flour is expected to be comprised of the grain endosperm and nutritional additives without extraneous material. If insects die and become fragmented inside grain kernels or grain bins, their skeletal remains are a form of extraneous material that can be difficult to find and measure. The current method of determining the amount of insect present is the fragment count. Insect fragments are located under a low powered microscope and counted. Concentration steps may be used prior to the fragment count to help insure that fragments are found (AACC International Method, 28-03.02). One way to concentrate insect fragments is to use floatation to separate them from the flour particles. Acid hydrolysis solubilizes starch to produce glucose or its short chain-soluble polymers. Allowing their removal by wet-sieving, leaving the non-starch components of the wheat and the insect fragments (AACC International Method, 28-41.03). Residual wheat or other plant material following a concentration step can be made translucent with a clearing method utilizing glycerin-alcohol (1 to 1) or clove oil to obscure the insoluble wheat material in order to allow insect fragments to show up better. Also, microscopists may choose to stain the insect fragments (AACC International Method, 28-03.02).

The material left after any of these possible treatments is traditionally spread over a grid section under a wide-field stereoscopic microscope to facilitate counting insect fragments.

During examination, large particles of wheat are turned over to reveal fragments that may be hiding underneath them. Non-distinguishable material may be mounted on a slide for further investigation with a compound microscope. The qualified microscopist requires knowledge and training concerning the components of wheat kernels and bodily remains of insects that may be in the wheat (AACC International Method, 28-03.02). For the tedious fragment count, it is a challenge to get reproducible results from the same microscopist. With different microscopists the results become subjective (Dogan and Subramanyam, 2017). Depending on handling, a single fragment can be subdivided resulting in a higher fragment count from the same fragment area. Brader et al. (2002) demonstrated that three different laboratories performing the fragment count correlated poorly with the actual number of insects in the sample. An ideal infestation determination method that measures the relative area of insect material in a field of view (FOV) would determine the amount of extraneous material independent of the insect bodily part and prior sample handling.

NIR imaging of organic binary mixtures enables the differentiation and the determination of the relative amount of the two distinctively different components of the mixture. This is true, provided there is a chemical contrast that exists between the entirety of the two components. The flour is high in starch whereas the insect fragments are high in chitin and protein, providing a detectable spectroscopic difference between the two materials. There have been attempts with limited success at using NIR spectroscopy to determine the extent of insect contamination in flour samples. An experiment where wheat kernels were spiked with adult weevils (Ridgway and Chambers, 1996) was able to determine when one kilogram of flour was spiked with 270 or more sawtoothed grain weevils (approximately twice the DAL). The same authors reported similar results with milled and whole grain samples. They determined the water content of the weevil

and the decrease in starch bands for the samples allowed chemical differentiation between grain and insect material once enough insect material was in the sample. No effort to determine the concentration level with immature weevils was reported, but they were able to distinguish sound kernels from kernels infested with weevil larvae and pupae. Perez-Mendoza et al. (2005) distinguished the number of fragments caused by the addition of kernels infested by lesser grain borers at different stages of maturity by the flotation fragment count applied to grain lots spiked with infested kernels. Fragment counts were performed on the flour milled from the spiked wheat to produce a plot of insects added versus the number of fragments found. An NIR calibration was based on the slope response plot versus the amount of insect added. The NIR results over a wide range (0 to 3 times the DAL) for each insect stage were linear, but when a sample concentration level was at or below the DAL of more or fewer than the 75 fragments per 50 grams of flour limit, the count was not reliable. The failure of the method is that the number of fragments does not account for the fragment area. These previous studies reveal the need to explore the potential of spectroscopic differences between flour and insect material.

Based on the analytical need, we initiated experiments to determine if localized NIR measurements of fragments in flour within an FOV could improve the accuracy and the detection limit based on local chemical distinction among the two components as opposed to one bulk NIR response. The imaging technique used divides the FOV into 81,920 localized pixels with a surface area of 40 μm by 40 μm. The discrete volumes where fragments are located in the FOV can have a large spectroscopic impact on an individual pixel, whereas a single spectrum for the FOV would obscure the response from the cross-section of insect fragments. Heterogeneity of a specimen was a potential hindrance to this approach for determining the relatively low amount of insect fragment in flour. The bran and endosperm of wheat kernels had different chemical

components. Different parts of the insect exoskeleton also differed in their chemical composition. Regions of the spectrum were selected to maximize the chemical difference between the insect and flour components irrespective of what portion of either of the two components occupy the pixels in the FOV. It was also necessary to employ uniform sample treatment while collecting spectroscopic data to avoid skewing results. From preliminary experimentation, it was readily apparent that the regulatory detection limits made it necessary to concentrate insect fragments present in the mixture prior to imaging. Much of Part II - Method Development is devoted to describing the experimental trial and error approach to sample preparation and treatment performed to solve the series of problems encountered while developing a practical fragment concentration method. The fragment concentration method removed a substantial portion of the starch by enzyme treatment followed by filtration. Finally, this included testing the method by spiking samples from a single commercial lot flour (King Arthur Flour Company Inc. lot number GAL0731) at progressively higher fragment concentration levels to mimic a commercially meaningful range of infestation. Subsequently all of the samples were then concentrated by the starch removal method developed and analyzed in order to test for reproducibility and linearity over the regulatory range. The results and conclusions are posted in Part III – Method Application. Prior to the method development and application, more introductory material is provided. In the next three sections, material over the chemical imaging instrumentation, previous chemical imaging applications, and spectroscopic features of insect and wheat flour components, are covered respectively.

1.2 - Near infrared imaging instrumentation

The spectroscopic imaging instrument used was designed to find the spatial locations and specific quantity of chemically pure aspirin, phenacetine, and caffeine (active ingredients) in

tablet dosage units for the pharmaceutical industry. Principle scientists (Dr. Linda Kidder and Dr. Neal Lewis) started the venture capital Spectral Dimensions Inc., (Olney, MD, USA) and developed commercial imaging instruments. The Sapphire® was the most advanced model. The optical diagram of the instrument is shown in Figure 1.1.

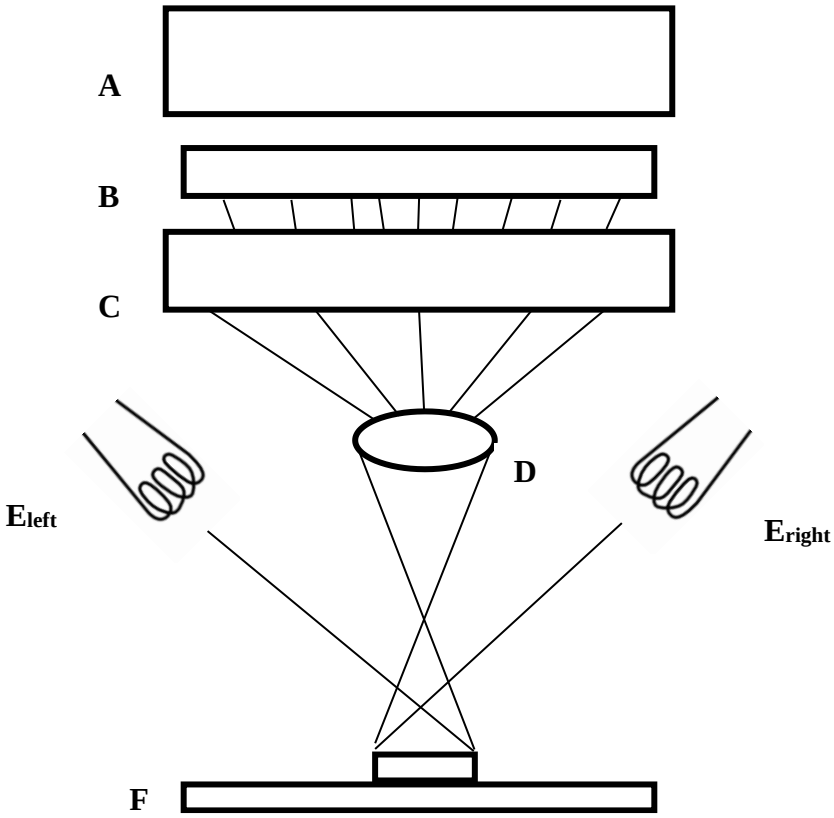

Figure 1.1 - Sapphire® NIR imaging instrument diagram

Electronics that control the liquid crystal tunable filter and monitors the focal plan array are represented with an (A). The focal plan array detector is represented with a (B). The LCTF that allows monochromatic light to hit the detector is represented with a (C). The lens that focuses the light onto the focal plan array is represented with a (D). The four tungsten source lamps are represented with (E_{left} and E_{right}). The stage on which the sample was placed is represented with an (F).

The Sapphire® used four quartz tungsten halogen lamps to uniformly illuminate the surface of a granular sample. The lamps are situated above at each corner of the sample stage so that diffusely reflected light can be collected by the microscope lens. The lens will then focus the collected light onto the solid-state detector array. In order to select the desirable wavelength of focused light, a liquid crystal tunable filter (LCTF) is operated between the lens and the detector. The focal plane array (FPA) detector is composed of thermoelectrically cooled indium antimonide (InSb) photodiodes, that have electromagnetic radiation sensitivity for most of the NIR region. A logarithmic sensitivity scale expressed as "D-star" values indicate the response of the solid-state detector from wavelengths 1000 to 6000 nm (InfraRed Associates Inc.). The FPA detector consists of 81,920 detector elements arranged in a rectangle of 256 by 320 elements; each individual detector element provides an image pixel that receives an individual response from the NIR radiation impinging on it. The LCTF can quickly be tuned to allow the desired wavelength to pass through allowing spectra to be collected. The number of scans and the collection time for each wavelength in the scan can be adjusted to achieve scanning speed while maintaining a high signal-to-noise ratio. The wavelengths can be selected by either scanning a range with desired incremental steps or by selecting individual wavelengths. The software provided with the instrument, using a spectra collection procedure designated as "wave table", enables select groups of wavelength ranges to be collected. This allowed the instrument to collect more data in informative regions, while avoiding the non-informative region between them. In this case the regions of 1680 to 1788 nm and 2020 to 2140 nm with a spectroscopic scan resolution of 3 nm in each region were used to provide analytically beneficial information. The region from 1790 to 2020 nm is omitted. Thus, more analytically useful data points were collected in each spectrum, improving the analysist's chance of success. Note that the

wavelength region skipped corresponds to the large water band at 1800 to 1950 nm which has been routinely excluded in the quantitative chemical imaging technique.

The Sapphire® required up to an hour of thermoelectrical cooling to minimize detector noise. By that time, the lamps have warmed up and the instrument will have run through a diagnostic check. After warm up, both a dark current (background) and a non-absorbing high reflective reference reading are collected. A deliberately out of focus, clean, polished, stainless steel mirror, which reflects the light source spectroscopically provided the dark current setting. A Spectralon® Fluorilon-99W^{TM} surface made of sintered polytetrafluoroethylene provided by Labsphere Inc. (North Sutton, NH) was used for the maximum reflective reference. Irregularities on the surface were minimized to make reflectance more uniform for each pixel. Unfortunately, when the decision was made to use a larger FOV to aid the filtration steps, a ceramic disc supplied by the same venders Labsphere Inc. (North Sutton, NH) that was large enough to cover the FOV had to be used. The ceramic disc also provided a high diffuse reflectance reference. The intensity of the incident radiation reaching each pixel in the FPA is stored for each wavelength. The reference radiation that is collected by the detector is preferentiality diffusely reflected radiation. After setting the zero and maximum reflection when sample images are collected the intensity of the radiation that has been detected for each pixel at each wavelength of the appropriate spectral range, the quotient of sample to reference intensity is calculated. This ratio is hereafter referred to as diffuse reflectance according to the definition in Applied Spectroscopy, "The ratio of the spectral intensity reflected by a scattering sample to that reflected by an equivalent non-absorbing reference that replaces the sample; sometimes refers to a measurement where spectroscopically reflected radiation has been prevented from reaching the detector." The mathematical equation is: $R = (I_S-I_D)/(I_R-I_D)$. Where R is the diffuse reflectance, I_S is sample

intensity, I_D is dark current intensity, and I_R is the reference radiation. The diffuse reflectance value is then expressed as $\log_{10}$ (1/R). This expression is similar to that of Absorbance (A) = $\log_{10}$ (1/T) in transmission spectroscopy (Applied Spectroscopy). The Beer-Lambert law also stated in Applied Spectroscopy explains that Absorbance (A) has a linear response to changes in the concentration (C) of the analyte when monochromatic light passes through a certain path length (b) of an absorber. Often and in this case NIR diffuse reflectance spectroscopy can use $\log_{10}$ (1/R) to achieve the same linear response in concentration of the absorber for wavelengths along a spectrum, so this expression will be called Absorbance from this point.

An imaged sample with the Sapphire instrument produces 81,920 individual spectra. One for each x, y location pixel of the FOV. A false color image indicates the Absorbance at each pixel for the selected wavelength, which can reveal the heterogeneity or uniformity of an individual functional group within the FOV of the collected sample.

To further utilize the massive amount of data, chemometric routines contained in the software provided with the Sapphire® instrument are applied to the sample FOVs. By collecting FOVs of pure component A (in this case insect skeletal remains) and pure component B (digested wheat flour) a massive number of pure spectra of each component can be stored in two "library" groups. The libraries for each of the components can be used to perform a partial least square (PLS) analysis to determine the percentage of insect material in each pixel of an FOV based on the spectral characteristics of the components found in each individual pixel. The image can then be viewed by a false color image that displays the relative percentage of component A or B in each pixel of the FOV. To calculate the relative concentration of A (insect area concentration) each pixel's PLS value of A and B are added together. The PLS value of A was divided by the sum of the A and B PLS values. The equation is:

$$\text{Relative composition of A} = \frac{A_{PLS}}{((A_{PLs}+B_{PLS})}.$$

This quantitation method enabled chemically distinct components to be determined without requiring a large amount of calibration data being analyzed. The pure component spectra enabled determination of relative composition of unknown mixtures. Another advantage was that spatial information on relative composition can be determined to gain information on the distribution of the components within an image. This aided in distinguishing components that represent a relatively low portion of the entire sample by distinguishing the few local areas where the foreign particles are present, provided the component's particle size is not too small compared to the pixels.

1.3 - Previous imaging applications in grains

Imaging has been a valuable tool for evaluating the quality of wheat. By the 1980s, Fulcher (1982) had already documented and used fluorescence microscopy to identify auto fluorescing components of cereal grains and utilized dyes to make components of interest fluoresce. The work showed that different parts of a wheat kernel have different fluorescing components. Pussayanawin et al. (1988) began by extracting ferulic acid (a fluorescent component found in wheat bran) using HPLC extraction. Their results led to the development of a method of determining the amount of ferulic acid that corresponded to the amount of bran in a wheat sample using fluorescent images of the sample (Pussayanawin et al., 1988). Imaging of the flour eliminated the need for an extraction and HPLC separation, to obtain the amount of ferulic acid, ultimately the amount of bran in the sample.

Other work using the Sapphire® instrument and the PLS method allowed a determination of endosperm content in flour in relation to the bran content. The goal of the flour miller is to maximize the recovery of the endosperm inside the kernel without pulverizing the bran into

powder. If done correctly, the miller can minimize the amount of bran in the flour by using size exclusion and density. Using NIR imaging and PLS to calculate the endosperm content has allowed tracking differences in the amount of endosperm released for different roll gap settings of the break system (Wetzel, 2013). In addition, in the milling process a purifier can help by allowing large chunks of endosperm to be further reduced while preventing similar-sized bran particles from being introduced into the flour stream. Use of NIR imaging to calculate endosperm content helped the experimental mill to maximize milling efficiency (Wetzel, Posner, Dogan, 2010). Another example of imaging being used to help the milling process was to track the migration of water into the wheat kernel during tempering. To track the tempering water, kernels were tempered with heavy water, water with the deuterium isotope of hydrogen, which altered the location of the water peak for the tempered water. Thus, collecting cross sectional pieces over different tempering times showed how far the heavy water traveled into the wheat kernel over time (Sweat, 1996).

Imaging using another instrument with an indium gallium arsenide (InGaAs) 320 by 256 FPA and an LCTF gave plant breeders a way to check wheat kernels for sprouting damage at the time of harvest (Smail et al., 2006). The effects of sprouting damage were further studied using mid-IR mapping of thin cross-sectional pieces of sprouted and non-sprouted kernels. The mapping in this case was done at the National Synchrotron Light Source of Brookhaven National Laboratory using a liquid nitrogen-cooled mercury cadmium telluride detector to catch confocally targeted light passing through the wheat cross section (Koc and Wetzel, 2007). Mapping allowed observations of localized changes in lipid and protein in the wheat scutellum, aleurone, and endosperm (Koc and Wetzel, 2007). The mid-IR instrument at the Synchrotron also helped researchers determine the secondary protein structure despite the massive amount of

starch in the cross-section (Bonwell et al., 2008). NIR imaging with the Sapphire® instrument has also been used to identify waxy wheat containing unusually high amounts of amylopectin in the endosperm (Dogan et al., 2008).

In a feed application, imaging helped determine mixing times for ingredient uniformity without adding extraneous ingredients into the formula that may not mimic mixing properties of the ingredients. Various different protein supplements are commonly added to ground cereals to make formula feeds. The uniformity within an FOV along with uniformity among FOVs was checked at set time intervals to find the least mixing time needed to achieve acceptable uniformity. Imaging can also distinguish among different protein sources to determine the effectiveness of mixing times, even if the chemistry of the components in the mixture was similar (Wetzel, Boatwright, Brewer, 2010).

1.4 - Spectroscopic features of insect parts, types, and life stages

In grain products, insect remains are considered extraneous material that reduce the value and wholesomeness of the grain product. The physical and chemical composition of the extraneous material (insect remains) and the grain gave hope that the two materials can be spectroscopically distinguished from each other, provided that the chemical differences between the components and chemical similarities within the components are sufficiently distinct and consistent. Prior to developing a method, chemical composition differences were analyzed over a variety of insect types, parts, and life stages. Three common insects to be fragmented in flour: *Tribolium confusum* (confused flour beetle), *Sitophilus oryzae* (rice weevil), and *Rhyzopertha dominica* (lesser grain borer) were obtained by maintaining colonies provided by the Grain Science Entomology Laboratory. Insects were killed by freezing and then sifted from the wheat kernels or flour. The collected insects were desiccated by ambient air flow for 24 hours. The

dried insects were finally fragmented with a mortar and pestle. The fragments were placed on top of the panchromatic highly reflective background of Fluorilon™ FW-99, a sintered Teflon surface with uniform pores of 25-35 microns provided by Labsphere Inc. (North Sutton, NH).

Preliminary spectra were collected on the Sapphire®, using the wavelength range of 1200 to 2400 nm with 10 nm intervals and with 10 scans coadded at each wavelength. The 2050 nm band was relatively pronounced for all insect parts due to the presence of N-acetyl-glucosamine, $C_8H_{13}O_5N$, which is a repeated sugar unit that is beta-1,4 linked to form chitin. Each sugar unit in chitin has an amino group with an N-acetyl group on the side-chain, which resulted in a well-defined amide band at 2050 nm. The protein band in the vicinity of 2160 nm was also prominent among insect fragments, but wheat flour had starch and gluten protein bands obscuring distinction at amide groups between flour and insect. Adult fragments with the previously mentioned characteristics are exhibited in Figures 1.2 through 1.4.

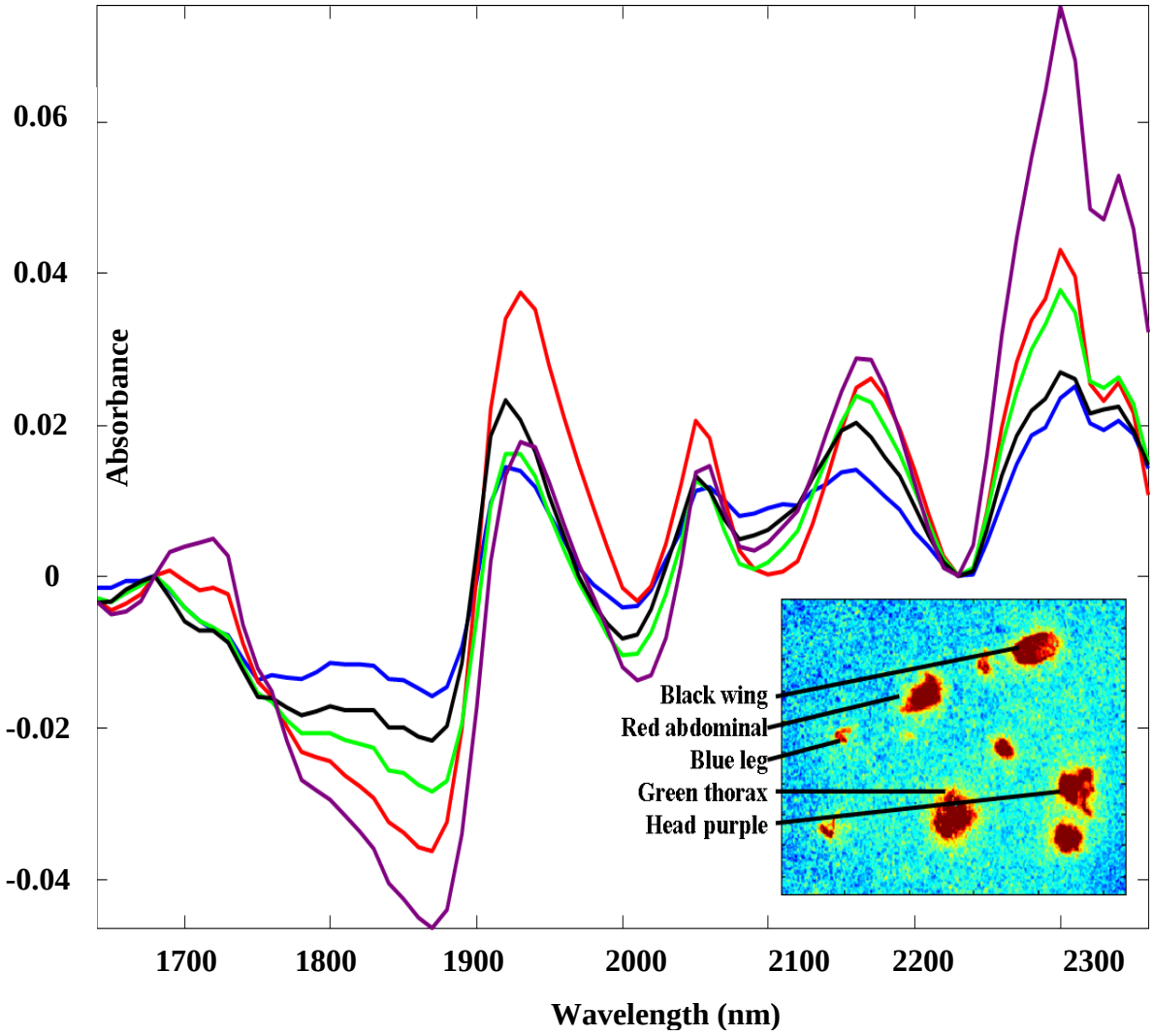

Figure 1.2 - Sitophilus oryzae spectra and false color image obtained by the Sapphire ®

A false color image is displayed of *Sitophilus oryzae* body parts placed on a neutral background of Fluorilon^{TM} FW-99. The false color images highlighted insect in bright red. Average spectra from 10 pixels are used to identify the characteristic absorption of wing (black), abdomen (red), leg (blue), thorax (green), and the head (purple). The thicker head and abdomen fragments of the *Sitophilus oryzae* had more intense bands at 1730 and 2050 nm compared to the thorax, wing and leg fragment. The wing fragment was the thinnest fragment, so it was surprising that it had more intensity than the leg fragment. The wing evidently had a higher lipid and chitin content compared to the leg. All the fragments have the chemical distinction for the

lipid and chitin content of the insect. Thickness and relative chemical composition of each fragment may change the relative strengths of the bands for different insect bodily part. Interestingly though, the wing (the thinnest part), has a high spectral response to the lipid and chitin. Thus, the thinness of the wing is compensated for by having relatively high lipid and chitin concentrations.

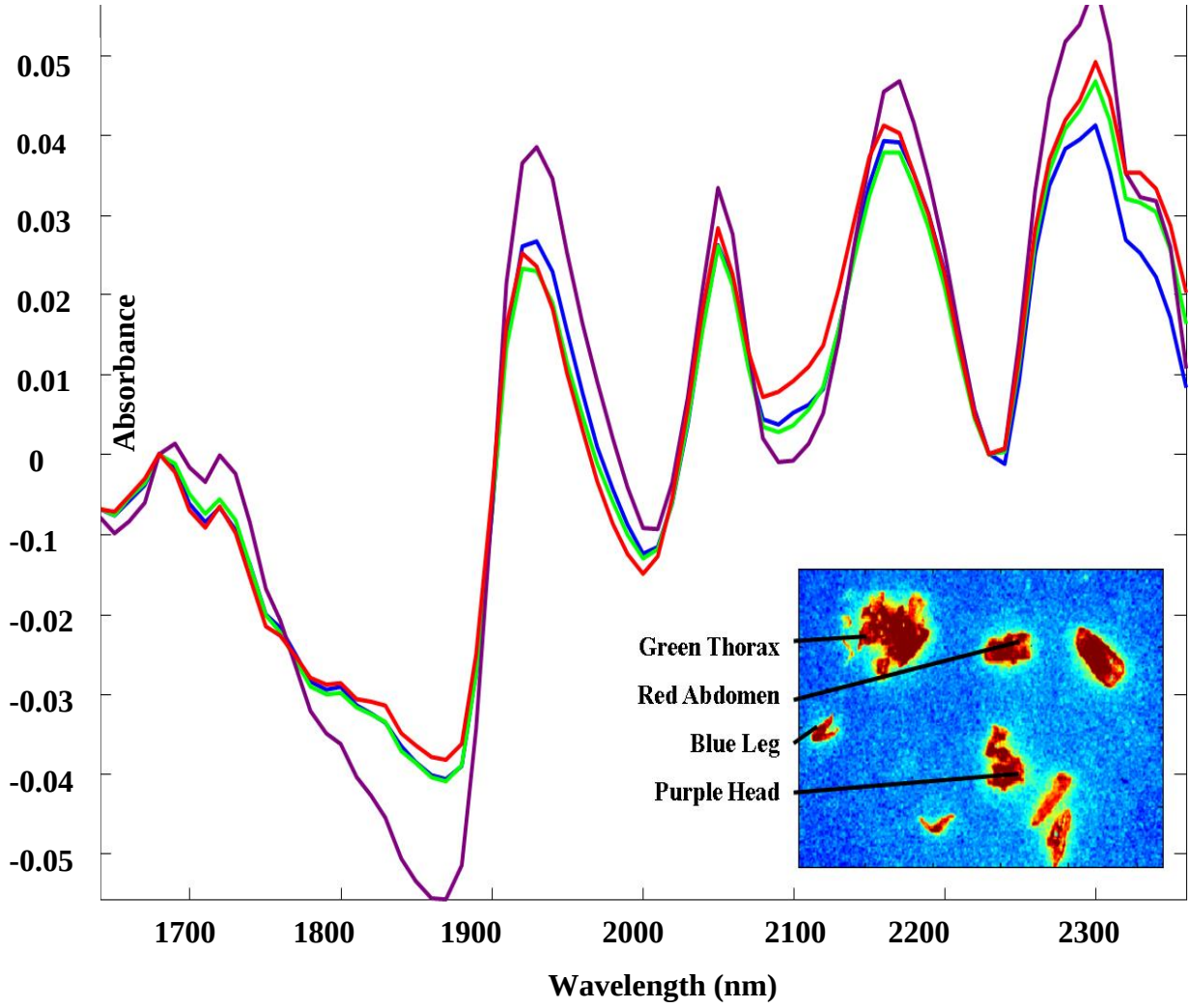

Figure 1.3 - Rhyzopertha dominica spectra and false color image obtained by the Sapphire®

False color images are displayed of *Rhyzopertha dominica* body parts placed on a background of Fluorilon^{TM} FW-99. The false color highlights insect with bright red. Average spectra from 10 pixels are used to show the characteristic absorption of thorax (green), abdomen

(red), leg (blue), and head (purple). The *Rhyzopertha dominica* spectra were more uniform in band intensity compared to the previous insect fragments. The 1730 and 2050 nm bands were prominent. The head fragment had more absorption, indicating a relatively high concentration of the insect lipid and chitin.

The *Tribolium confusum* is shown at immature stages along with a few fragments at the adult stage in Figure 1.4.

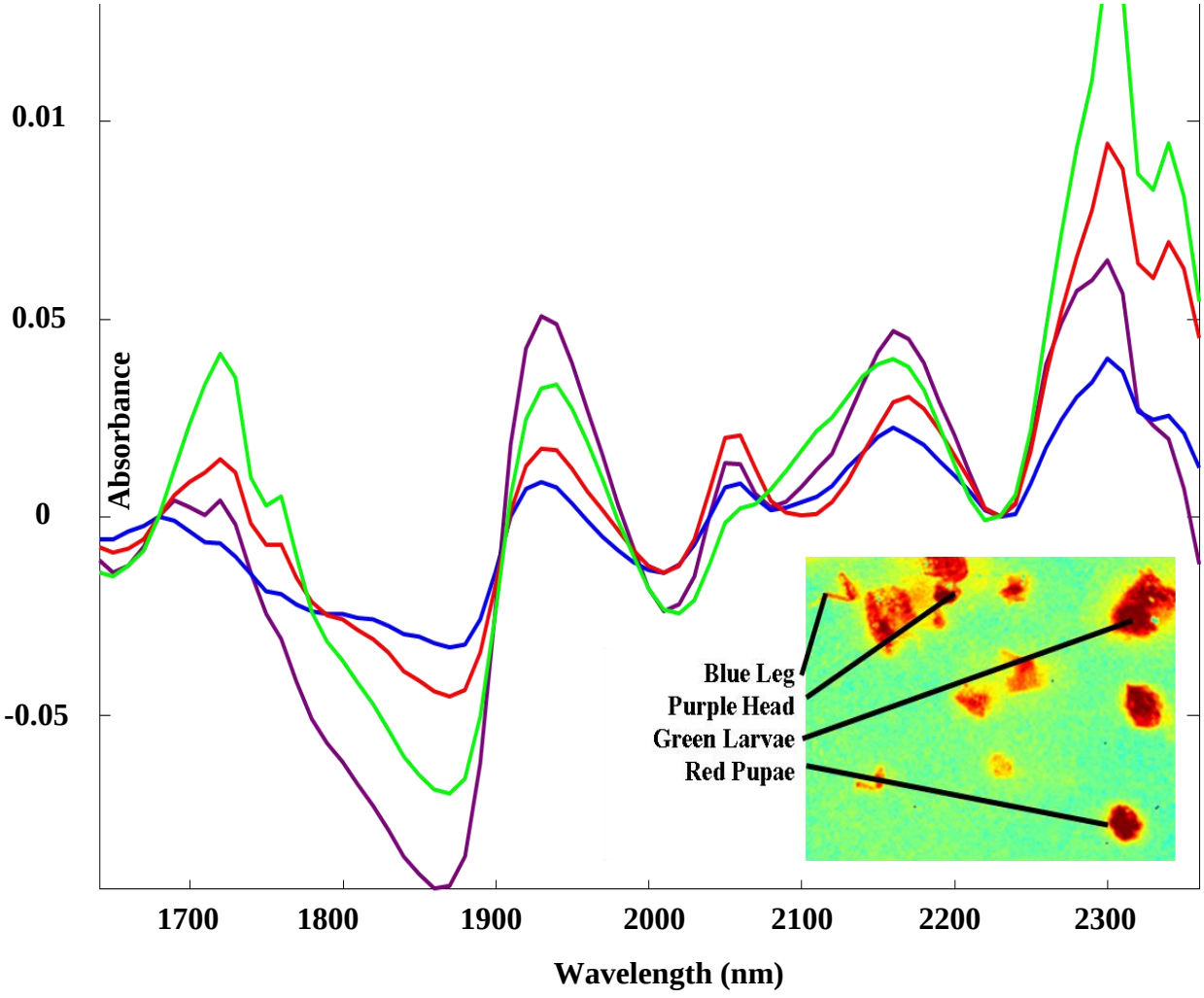

Figure 1.4 - Tribolium confusum spectra and false color image obtained by the Sapphire ®

A false color image is displayed of *Tribolium confusum* insects at all life stages. The false color highlighted insect material with bright red. Average spectra of 10 pixels are used to show

the characteristic absorption of leg (blue), head (purple), larvae (green), and pupae (red). The spectra of immature fragments looked very similar to those corresponding to adult insects. Larvae had a large absorption band at 2180 for protein. It also had the chitin peak at 2050nm, but it was less pronounced. The pupae piece had a diminished protein band and a prominent chitin band. In fact, the pupae fragment had a higher chitin band than the leg. The larvae had the highest 1730 nm lipid band among the 4 fragments, revealing that the pupae had a high quantity of lipid and protein. At each life cycle the same chemical components resulted in the same bands among each insect type, and body part. At the adult stage, relative concentrations appeared fairly uniform, with the wing and head having elevated chitin and lipid content. Fragments from the pupae stage appeared to have enough chitin and lipid to be distinguished as readily as those in adult fragments. Larvae fragments had a good chance of being distinguished by the 1730 nm band due to them having a lot of protein, but the 2050 nm chitin band may be obscured very easily in the presence of flour.

So far, the insect similarities have been examined, but the flour base was also important to distinguish insect fragments. High quality bread baking flour contains largely starch, therefore the (CHO) group showed a strong broad band at 2100 nm, with a small protein band at 2180 nm assigned to the NH stretch for the amide group causing a shoulder on this band. The contribution of protein absorption bands from both the insect fragments and the flour made the region less reliable in distinguishing insect material from flour. Regardless of insect part, the 1730-1750 nm and 2050 nm bands were superimposed on to the flour spectrum. Figure 1.5 shows the coadded spectrum of the flour and the spectrum of insect parts on top of the flour.

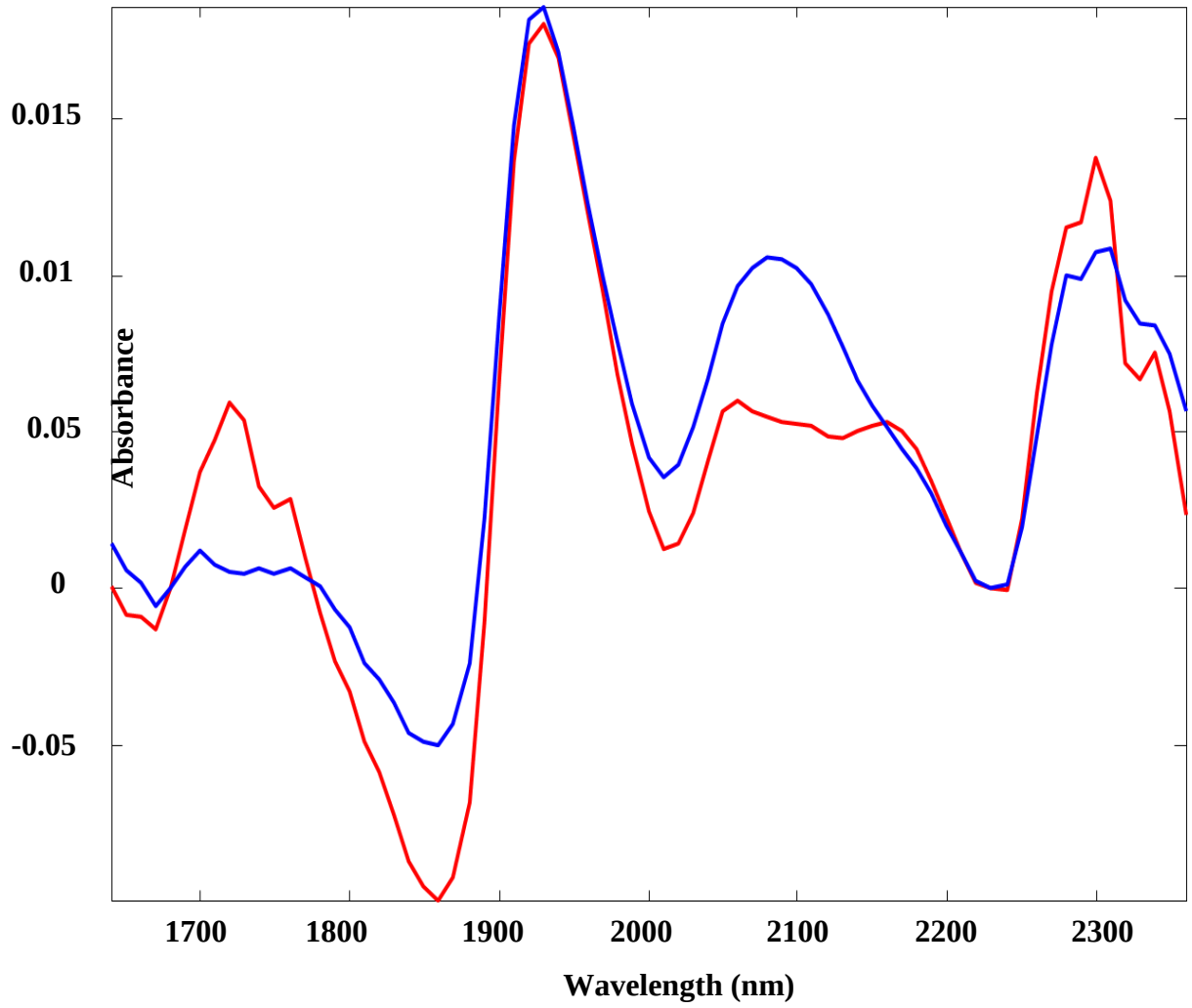

Figure 1.5 - NIR spectra of flour and insects

The red spectrum is that of the coadded insect spectrum on the flour surface. The blue is that of the coadded spectrum of the flour background. The 1730 and 1750 nm bands were very prominent compared to the flour spectrum. The 1750 nm absorption was not prominent on the Fluorilon^{TM} FW-99, but it was once fragments that were placed on flour. The 2050 nm band for chitin is still distinguished, but the flour 2100 nm starch band is broad and will quickly cover the insect spectrum if the fragment was below the surface.

Part 2 - Quantitative insect fragment method development

2.1 - Optimizing NIR imaging

To maximize the potential for spectroscopic distinction with the Sapphire® instrument, portions of the spectrum were identified that best discriminated insect fragments from flour. The instrument's software enabled the collection of only the most useful wavelengths within the limited number of wavelengths that can be collected for one image. After finding wavelengths that discriminated insect fragments from wheat flour, samples were tested for heat degradation to determine if the resident time of the sample on the stage prior to analyzation needed to be restricted. Also, the effect of optical penetration of the material in response to pressure exerted upon the specimens during the collection of spectrum was tested.

2.1.1 - Discriminating NIR wavelength selection

The region of 1200 to 2400 nm was first collected using the Sapphire® to compare the spectrum of each insect component to find regions that distinguish insect bands in the presence of wheat flour spectra. Once the spectroscopic regions that were helpful were identified, the non-informative regions were ignored while performing the analyses. The 1680-1788 nm region distinguished lipid and protein from the insect exoskeleton from both the carbohydrate and cellulose of the wheat flour. The 2020-2140 region contained a band for insect chitin. The chitin region enabled identification of even thin insect fragments on the surface of the sample. However, the strong CHO band for starch is near the chitin peak and may obscure the chitin peak when the fragment is very thin or covered. Wheat endosperm on the surface could absorb enough electromagnetic radiation to prevent chitin from insect fragment underneath from being spectroscopically detected. Fortunately, the lipid and protein region (1680-1788 nm), appeared to

reveal submerged and thin wing pieces that did not have a pronounced chitin band. The drawback of the region 1680-1788 nm was that the thick pieces of insect fragment did not show up to the extent that they did with the chitin region. There were three options in which spectra could have been collected. The first option was to collect the chitin region in order to make the most of fragments that are thick and near the surface. The second option was to collect the protein and lipid region to discern thin and submerged fragments while not having the greatest response on thick surface insect fragments. The third option was to collect spectra at each region, but the increment of wavelengths collected would have to increase, because there was a limit to the number of wavelengths that can be collected in one image. An image of a fragment was collected three times: once at the 1680 to 1788 nm region with a 1 nm spectral resolution, once at the 2020 to 2140 nm region with a 1 nm spectral resolution, and once at both regions with a 3 nm spectral resolution. The two regions combined worked best to quantitate the presence of insect in the sample, because they worked together to overcome situations were each region had trouble determining insect concentration.

Wheat gluten, which was not a large component of the flour, had a band at 2060 nm. The normally low concentration of gluten in flour was increased by the concentration steps used by reducing the starch content. This caused the concentrated wheat flour and insect chitin spectra to be similar; fortunately, differentiation of the two components is still possible. Figures 2.1 and 2.2 revealed spectroscopic differences between concentrated flour and insect material. Concentrating the sample reduced the chemical distinction between the insect exoskeleton and wheat flour, but the difference was sufficient for a useful PLS calculation. Results revealed that chitin bands were distinct from the gluten band even for very thin pieces of leg or antenna.

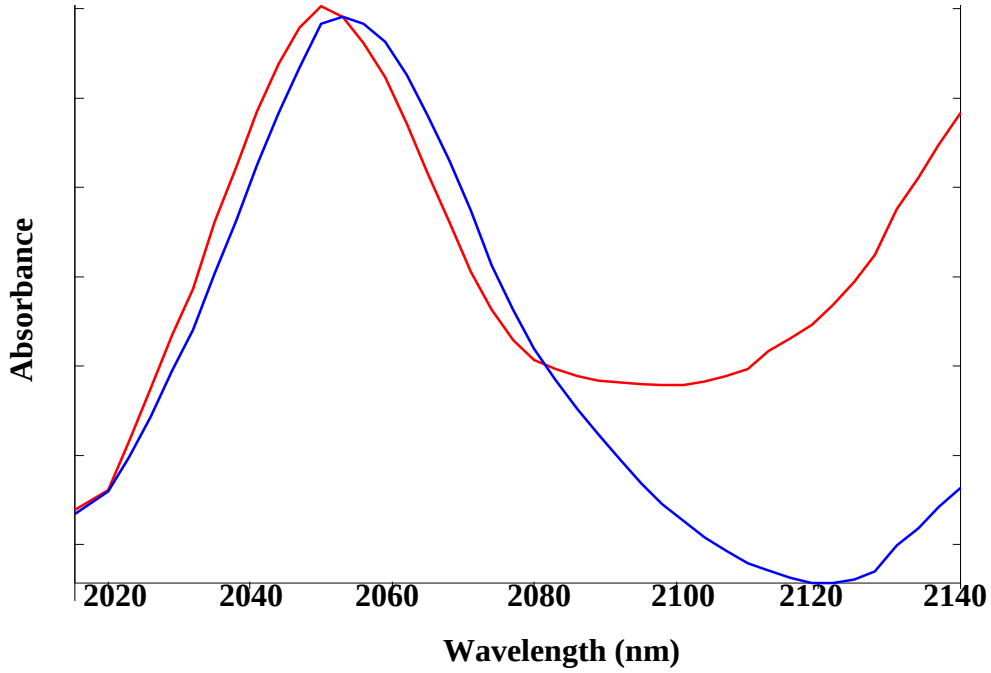

Figure 2.1 - 2020 to 2140 nm region of insect (red) and concentrated flour (blue)

The bands had slightly offset peaks with the insect spectrum centered on the 2050 nm peak.

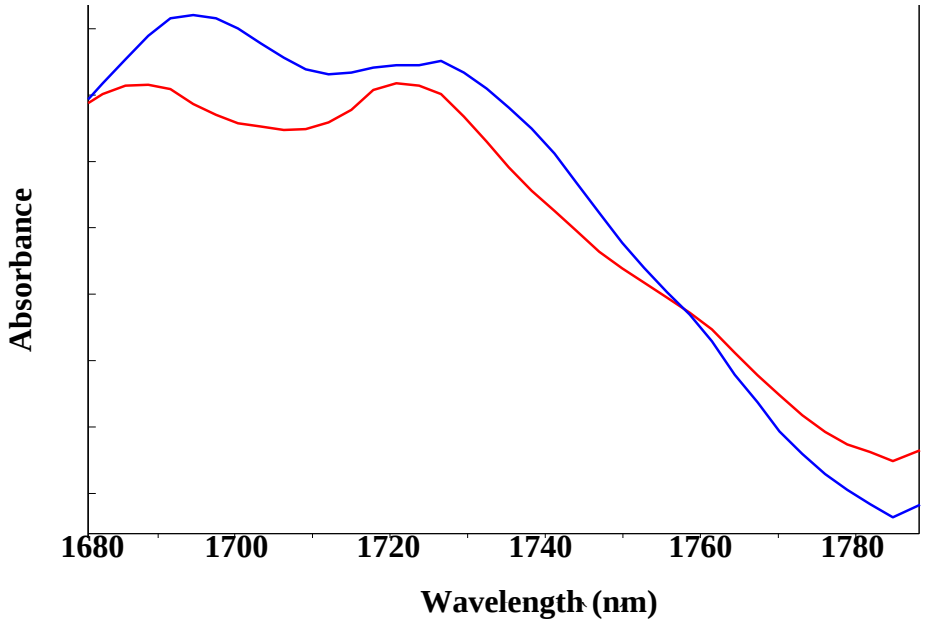

Figure 2.2 - 1680 to 1788 nm region of insect (red) and concentrated flour (blue)

The bands had slightly different shapes for insect and concentrated flour.

2.1.2 - Checking for effects of heat degradation

During NIR analysis, the absorption of electromagnetic radiation produced vigorous vibrational and rotational motion in the sample of bonded atoms, resulting in heat. Protein structure can change from the heating of the sample while the spectra are being collected. If bonds were broken, they can no longer absorb energy from the electromagnetic spectrum; if secondary or tertiary protein structures changed under heat, the band itself may shift or change intensity. To discover how heat effects the identification of insect fragments, several images were collected in succession on top of Fluorilon^{TM} FW-99. One specimen had intervals of 45 seconds between image collection to allow heat to dissipate while each image is produced. The other test had 90 seconds of recovery time to allow heat to dissipate before each successive image collection. The spectra of individual pixels were examined quantitatively by PLS analysis to identify the insects on the surface. The spectra were collected from 1540-2400 nm with 10 nm increments. The spectra were baseline corrected at 2020 nm and 2400 nm and the water band from 1850-2000 nm was masked. First figure 2.3 shows the spectra of the short 45 second recovery time.

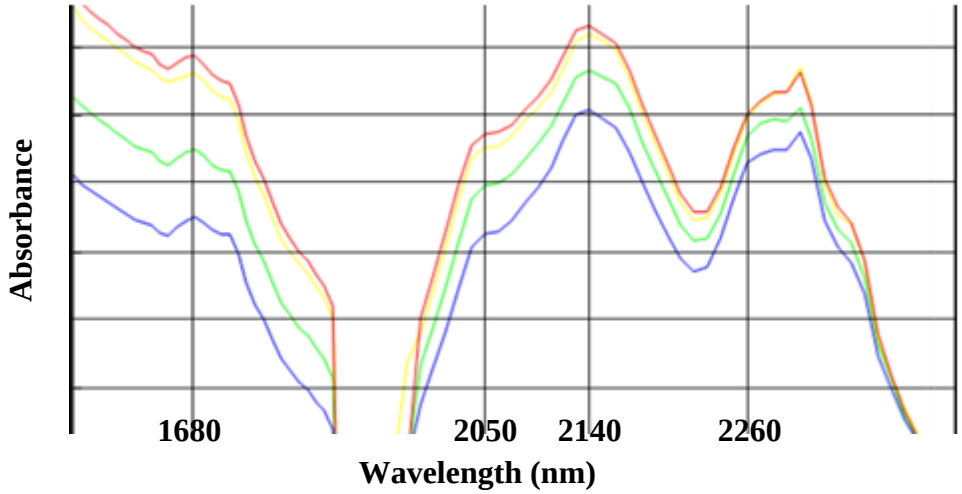

Figure 2.3 - Spectral heating effects with a 45 second recovery time between NIR spectra collection

The blue spectrum was the average of the spectra over an insect fragment from the first image. The green spectrum was from the second image. The yellow spectrum was from the third image and the red spectrum was from the fourth image collected. The 1680 and 1700 nm absorption band heights did not change relative to the base of the bands. The bands in the 2000-2400 nm region appeared to have an increase. The 2260 and 2300 nm increase was very slight. These bands were subsequently not included, because they were not helpful in determination of insect fragment concentration in flour. The ratio of band heights 2050 and 2140 nm was respectively a ratio of chitin to protein, and this ratio increased at a diminishing rate with each image collected. It was a slight increase, but it may indicate a denaturing of protein in a way that decreased the effect of the functional NH groups in the amino acids of the insect protein, while the chitin was resistant to the heat. The overall intensity increased at a diminished rate with each successive spectral image, indicating that the heated specimen absorbed radiation slightly better, but spectroscopic characteristics were not altered except for the 2140 nm peak. Next the 2000 to 2400 nm region of the average spectra of an insect fragment with the 90 second recovery time is shown (Figure 2.4).

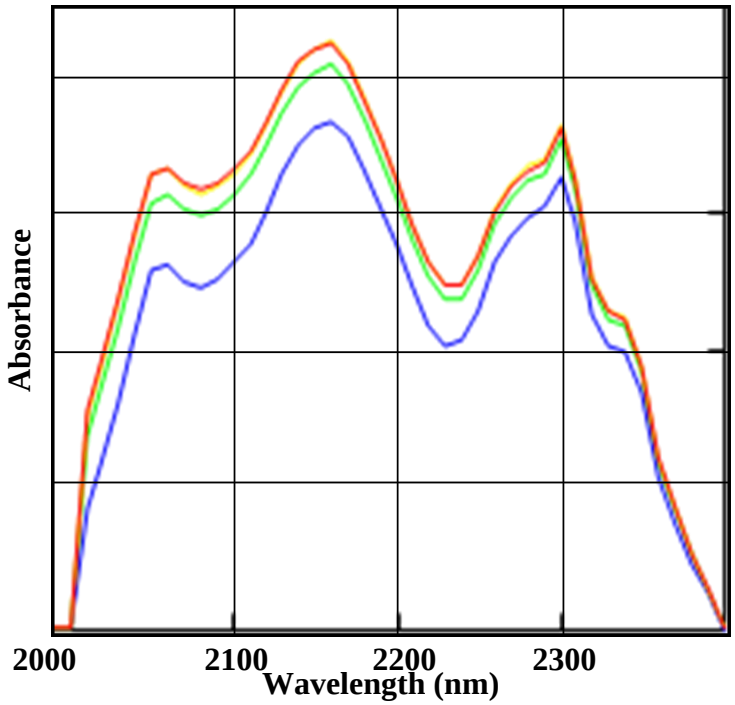

Figure 2.4 - Heating effects with a 90 second recovery time between NIR spectra collection

The blue spectrum was the average of the spectra over an insect fragment from the first image. The green spectrum was from the second image. The yellow spectrum was from the third image and the red spectrum was from the fourth image collected. The longer time between 180 second image collection allowed the sample to cool down so the increase in absorption was less across the spectrum. The ratio of 2050 to 2140 nm also increased at a diminishing rate. The same protein denaturation was present after the protein cooled down between each image collection, strengthening the idea that the protein was denatured by the heating during the image collection, rather than vibrational energy in the bonds being saturated if the image was collected after the sample had already been heated from the radiation of the instrument's lamps.

The effect of heating and therefore denaturation of protein did not alter the ability to classify and determine of the percent area of insect fragments on the flour surface. PLS analysis was performed using a specially constituted component library consisting of insect fragments for

one component at the time. Fluorilon™ FW-99 for the other component. Figure 2.5 shows the false color images applied to the PLS scores.

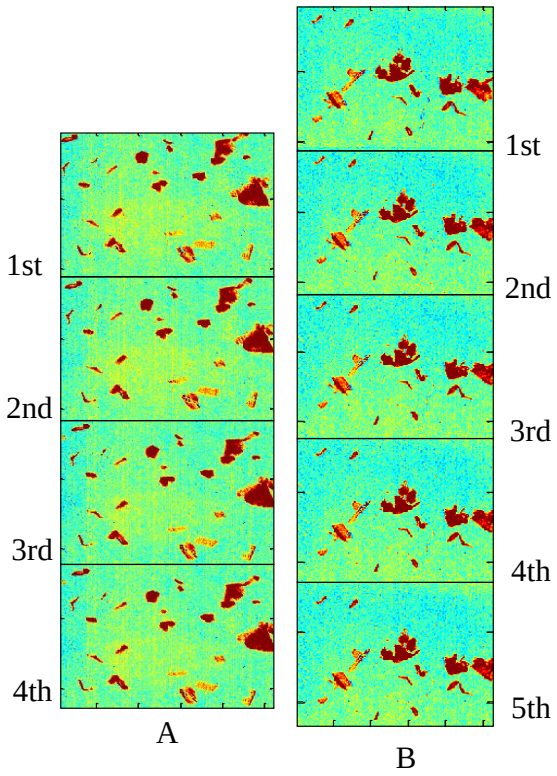

Figure 2.5 - Chemical distinction of successive images with intermittent rest time

Column A of the figure contains images from the same sample collected for 180 seconds consecutively with a 45 second rest between each image, and column B of the figure contains images from another sample collected consecutively with a 90 second rest between each sample. The rest period allowed heat to dissipate between each image collection. Column A had a mean result of 7.9% with the largest deviation from the mean at only 0.3%. Stack B had a mean result of 7.3% with the largest deviation from the mean at only 0.2%.

2.1.3 - Optical response to granular compaction

Pressure application that packs the sample closer together affects the depth of NIR radiation penetration below the sample surface. Penetration depth alters the collected spectra

enough to change the measurements for components of interest. After determining that chemical changes from heating did not affect the determination of insect fragments optical responses were measured on images at successively higher pressures to see if increasing pressure and thereby compression changes the measurement of imaged insect fragments. Images collected from the same specimen at three different pressure levels are shown in Figure 2.6. The pressure was increased by placing a cover glass over the sample and adding lead weights to the cover glass in an arrangement that did to not block the sample. The PLS score changed little with increased pressure, but when the pressure increased, the edges of the insect fragments appeared less well defined. Because of these results, subsequent the specimens were not routinely compressed during spectroscopic analysis.

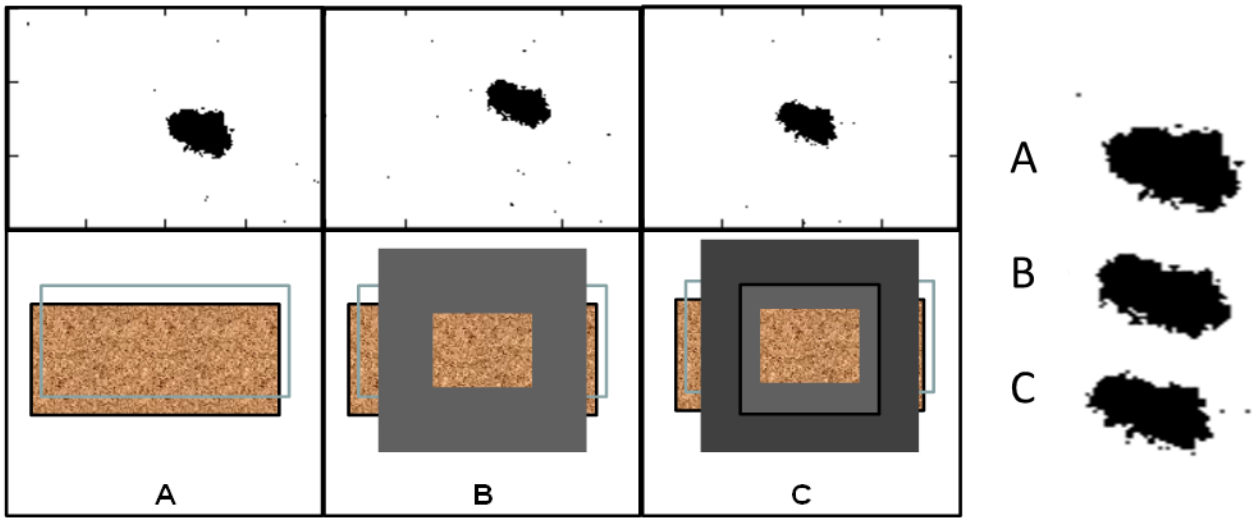

Figure 2.6 - Chemical distinction of insect fragment at three levels of pressure

These images were collected at increasing applied pressure. The first image had a glass microscope slide over it. The second had a single lead weight with a hole in the middle to keep from blocking the FOV. The third had a second lead weight on top with a slightly larger open area. To the right the insect fragment was magnified to show the decrease in chemical distinction along the edges.

The spectral window used to distinguish the insect fragments from the flour was further reduced for the final experiments. The average spectrum over the insect, and the average spectrum over a similar size of the flour are shown in Figure 2.7. The region from 1680 to 1788 nm remained distinct and unchanged with increased pressure. The 2050 nm absorption band was obscured with increased pressure, but not totally obscured to the flour's starch band. Normally, pressure is expected to pack particles and take away gaps encountered in the light path. Compaction decreased the effective path length. It was anticipated that a decrease in spectroscopic intensity, would occur. Compaction increases with pressure, but the starch present under the fragment appeared in the spectra more as pressure was increased. The loss of fragment edge resolution did not result in a large calculated loss of percent insect area in the flour.

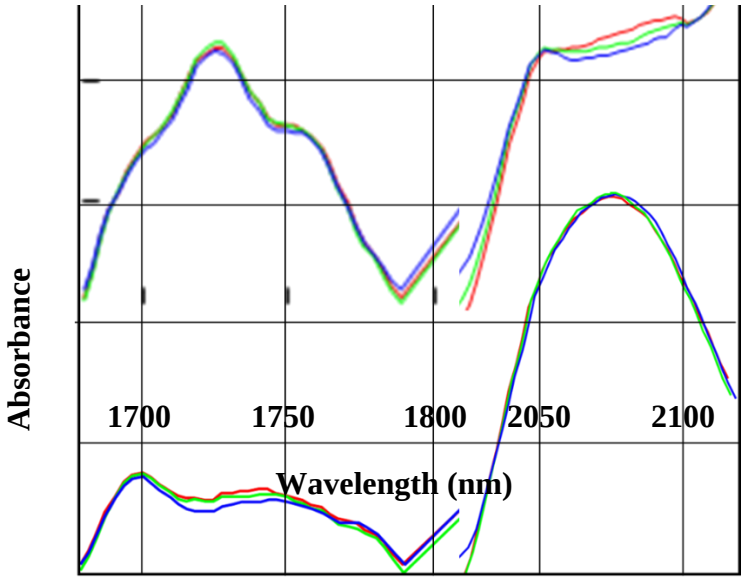

Figure 2.7 - Spectroscopic effects of pressure

Top spectra of insect fragment: blue 1x pressure, green 4.5x pressure, and red 7.4x the pressure. Bottom spectra of flour with the same color scheme for denoting different applied pressure. From these spectra and their results, pressure was not added to the sample because it apparently did not help identify insect fragments in flour. In fact, pressure decreased the

classification of insect fragments on the thin edge pieces. Increased pressure makes the starch band more prominent, obscuring the chitin band enough to alter the quantitation of insect detection in samples that are tested in a regulatory meaningful range.

2.2 - Specimen concentration

The fragment count was converted into parts per thousand (ppt) by weight of insect material in flour by weight. Initially several adult *Tribolium confusum* were weighed to obtain an average weight. The average weight of an adult insect was 1.27 mg. A round number of fragments was used, 10 fragments per insect. Dividing the average insect weight by 10 and multiplying that by 75 caused the total weight of the insect fragment at the DAL of 75 fragments per 50 g of flour to be 9.53 mg. This defined fragment weight was converted to a concentration of 0.19 ppt of insect material in flour by weight. In order to image a sample with the insect material in a distinguishable range, concentrating the fragments in a sample was necessary.

Concentration by particle size appeared to be the logical first step in concentrating the insect material present in the bulk sample. The bran and insect skeleton were not as friable as endosperm. Therefore, a large portion of the flour in a sample could be removed by simply sieving and retaining the overs of the sieve. After physically concentrating the sample by particle size, it needed to be further concentrated by starch digestion. The quickest and most complete way to remove the starch would be by hydrochloric acid starch digestion. Acid hydrolysis was rejected based upon its corrosive damage hazard.

The enzyme α-amylase can alternately digest starch in a similar amount of time when using a heat-stable α-amylase. The fungal α-amylase soluble digestate needed to be separated from the insect material. After numerous trial and error attempts it was apparent that a nylon cloth filter surface needed to be physically cleared of residual slurry by rubbing a glass rod over

the filtering surface. The liquid in the sample from enzymatic concentration was removed, but the residual sample needed to be formed into a smaller filter cake for imaging. A complete step by step procedure is located in Appendix A on page 65.

2.2.1 - Physical concentration

Flour for human consumption in the United States is defined, by law, to allow 98% of its material to pass through a 212 µm opening (sieve # 70), although the flour actually contains a range of sizes below that level (Sec. 137.105 Flour, Title 2). Wheat bran typically is on the larger end of the particle size distribution. In contrast the insect fragments tend to be larger than flour particles: and have a tough, yet pliable, exoskeleton that fractures at the joints or in the middle of long pieces of exoskeleton. Insect fragments obtained from desiccated insects that were placed in a glass jar with glass beads and shaken were examined under a microscope. Most fragments were longer than 150 µm in one dimension at least. Experimentation revealed that insect fragments themselves remain over a sieve with 150 µm openings, whereas the sieve can remove 90 to 95% of a flour sample in the same experiment. The concentration time that a sample required and the flour quantity removed were both determined using a 150 µm opening sieve in a Ro-tap assembly configured for this purpose.

Initially 2 minutes of sieving with, a Ro-tap assembly concentrated the sample by a factor of 10 to 13 and retained the insect fragments as overs of the sieve. However, the concentration step was insufficient. After the physical particle size concentration α-amylase hydrolysis of starch was used to further concentrate the insect fragments.

2.2.2 - Fragment concentration by α-amylase hydrolysis starch removal

To further concentrate the sample after physical sieving, a method was sought to chemically concentrate the fragments by starch hydrolysis solubilization. α-amylase was used to hydrolyze starch to produce soluble sugars or short polysaccharides. Enzymatic digestion is most efficient when heated in water to 80°C. The objective was to optimize the rate of digestion without denaturing the enzyme.

After preliminary experimentation 75 minutes of reaction time at 80°C was selected to provide complete digestion. After 75 minutes, digestion was terminated promptly by placing the digestion tube in boiling water for 5 minutes. The heat denatured the enzyme, terminating hydrolysis. The resulting digestate contained a mixture of water, denatured gluten and enzyme, digested flour consisting of dissolved sugars, small polysaccharides, and cellulose.

2.2.3 - Filtering the specimen

Water aspiration provided suction for filtering the digestate. A trap flask was placed between the filter assembly and the water aspirator to avoid tap water from backing up into the collected filtrate.

A number 8 rubber stopper with two holes was placed on the Suction flask: one hole provided a line to the actual suction flask, while the other hole had a bleed valve to apply or break the vacuum. A diagram of the suction flask and filter assembly is shown in Figure 2.8. Four filtering systems were attempted before obtaining a working solution. These attempts along with their failures will be explained.

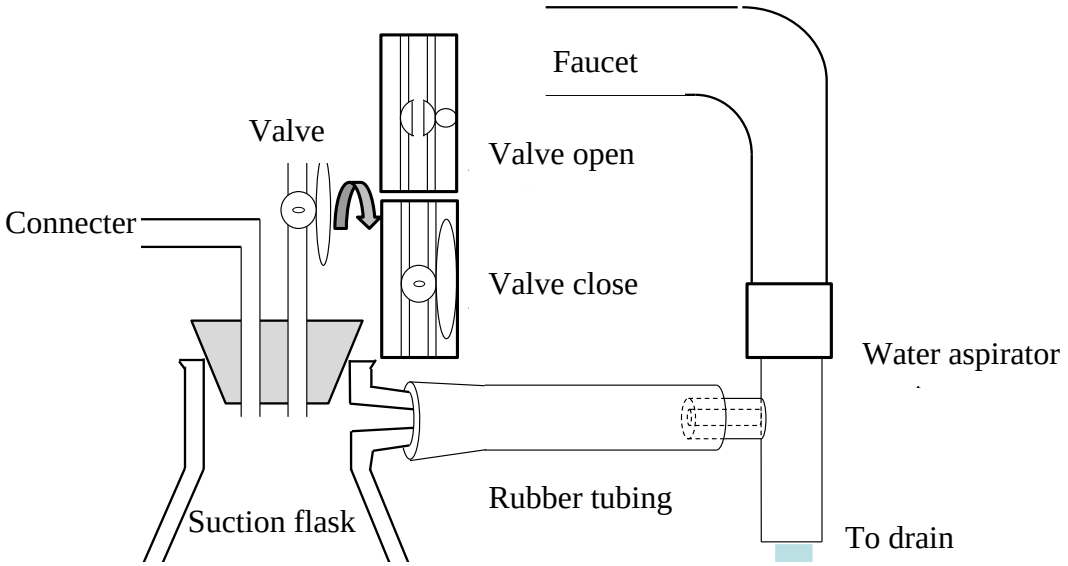

Figure 2.8 - Water aspirator and trap flask

Trap assembly between suction filter and water aspirator flask was used to protect the filtrate. A stopcock was used to allow atmospheric air into the trap.

First, an attempt used a porcelain Buchner filter funnel (product number 5212B10, Thermo Scientific, Swedesboro, NJ) to support grade 1 filter paper. Figure 2.9 shows this filtering system. The porcelain funnel had a diameter of 14.5 mm and depth of 8.5 mm with 1 mm holes over the filtering surface. The funnel spout went through a number 8 rubber stopper that fit into the suction flask. After hours of suction, only a small amount of filtrate had accumulated in the suction flask due to a build-up of the filter cake that increased resistance to the filtrate flow.

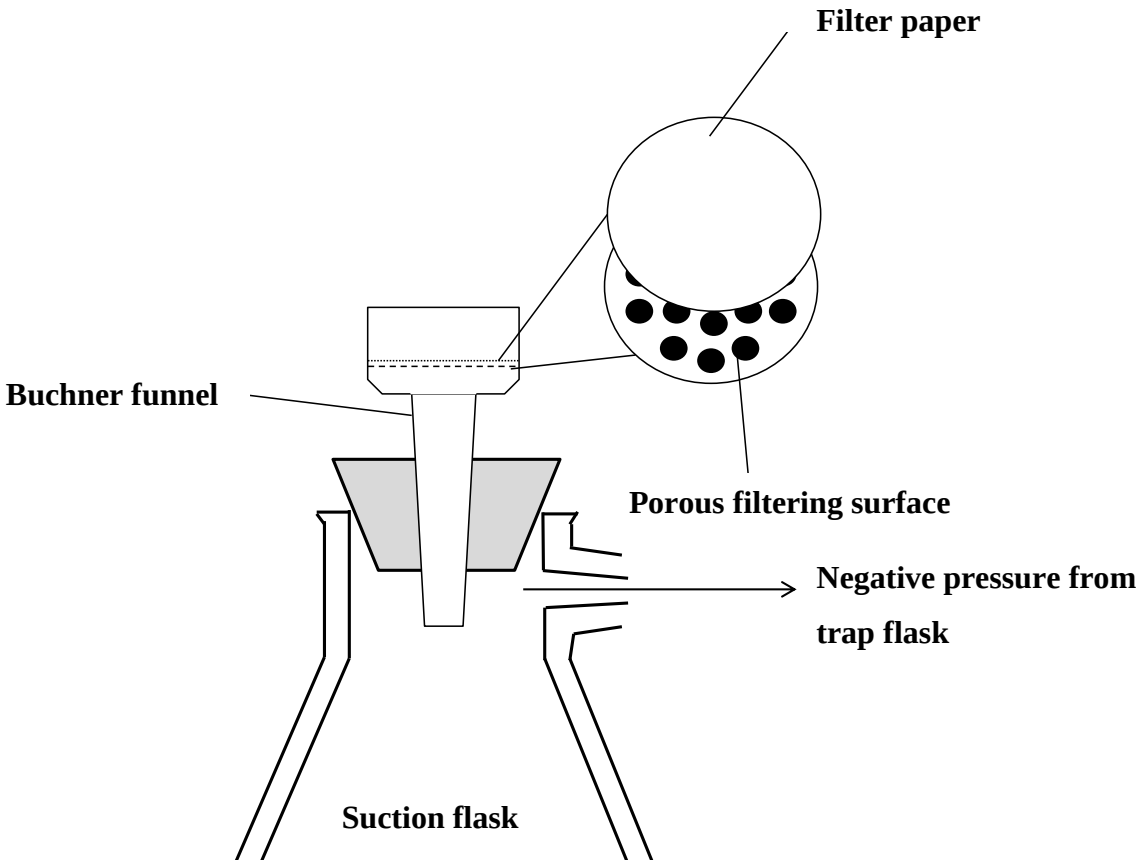

Figure 2.9 - First filtering attempts

The first filtering apparatus was a demountable Buchner funnel with an 11 mm diameter filtering surface to support grade 1 filter paper. To avoid the thick solid filter cake deposition an 83 mm diameter filter paper supported with a larger diameter porcelain Buchner filter funnel (product number B212B40, Thermo Scientific, Swedesboro, NJ) was used. The funnel was 83 mm in diameter and 39 mm deep to provide a larger filtering capacity. The flat surface of the funnel was 60 mm in diameter with 1 mm diameter holes. Even with the 60 mm diameter filter the process exceeded an hour. With either size filtering surface, the undissolved portion of the wheat flour quickly clogged the pores of the filter paper, preventing most filtrate to pass into the suction flask. After only a few minutes, the filtration process slowed to the point that after an hour very little liquid was pulled from the sample. Most of that liquid passed through in the first few minutes of the process.

For the third attempt a filtering surface was used that had more, but smaller, pores that allowed suction to be applied uniformly over the entire diameter of the filtering surface. An EMD Millipore brand glass filter assembly (catalogue number XX1004700, Merck KGaA, Darmstadt, Germany) was used. That assembly included a 300 mL capacity glass funnel, with a 47 mm fritted glass filter placed in a number 8 rubber stopper. A spring clamp secured the demountable funnel to its base. (Figure 2.10) The filtration area of the coarse fritted glass was 33.5 mm in diameter. Unfortunately, the high porosity of the filter support still did not reduce filtration time because the slurry of digested wheat flour clogged the pores very quickly.

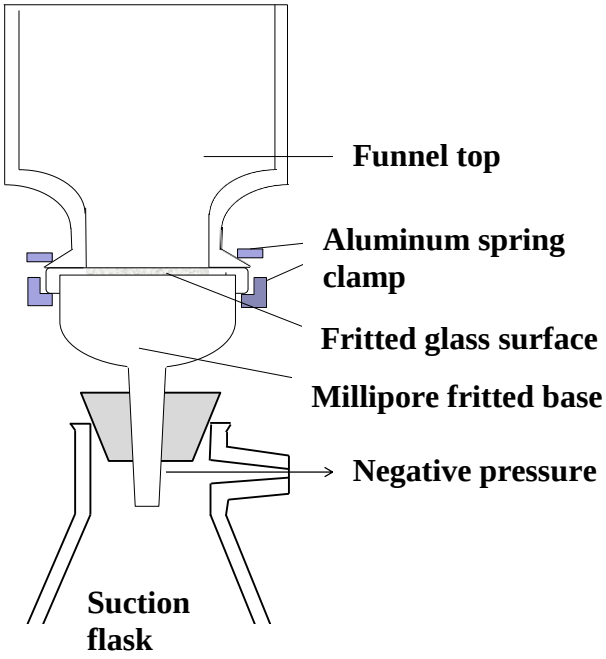

Figure 2.10 - Third filtering attempt scheme

The third attempt at filtration used an EMD Millipore glass filter holder assembly for increased porosity, but it did not speed up the process. The fourth attempt used the same Millipore brand funnel top, but without the base. Instead, the funnel was placed directly on top of the filtering flask. The same filtration area of the Millipore filter assembly was retained, but 130 µm opening nylon bolting cloth was cut into a 7.7 cm square and placed between the filter funnel assembly and the suction flask. The bolting cloth provided a greater open area over the same filtration diameter. The top of the flask was flattened by sanding with fine grit Carborundum abrasive paper supported by flat glass plates. To provide a tighter seal and to hold the cloth firmly in place, a gasket was made by cutting a donut shape out of a white flat rubber stopper

designed for a bathtub or sink to fit the inner and outer diameter of the flat ground glass opening of the suction flask. Because the mouth of the suction flask did not fit into the aluminum clamp of the Millipore assembly, rubber tubing was cut into four 1-inch long pieces. Each piece was cut along the length. Each of the four cut pieces could be placed on each of the clamp jaws. The fabricated assembly worked to secure the flask and funnel together. The homemade rubber gasket prevented the whole screen from being sucked into the flask. Regrettably the increased open area of the filtration surface still did not result in a practical filtration period. In fact, it still took hours for the filtrate to be separated from the sample. Even adding salt to reduce the ionic strength in the wet proteins to allow water to more easily pass through did not help (Hyde et al., 2017). The surfactant Tween 80 was also used in the hope that it could interact with hydrophobic portions of the protein to reduce interaction. The process did not allow the liquid to filter through the solid material any easier (Johnson, 2016). The proteins appeared to stick together thereby clogging the openings of the sieving cloth. However, this system was not discarded, but modified to mimic the Glutomatic method designed to isolate wheat gluten.

The Glutomatic method of determining gluten strength presumably had a similar concern in isolating protein in flour samples. The gluten method first mixed water, salt, and flour to develop a gluten matrix (Perten Instruments, 2015). The starch is separated from the gluten by rinsing samples with a salt water solution while the samples are stirred over an 88-micrometer opening polyester sieve (Perten Instruments, The Glutomatic System Operation Manual). In this procedure, the bars that stir the sample also rub against the sieve itself, to prevent clogging.

Similar to the Glutomatic method, a glass rod was continuously and gently rubbed against the surface of the 130 µm opening sieve during filtration. This process allowed water to be rapidly separated from the solid specimens. The solid residue was then rinsed a second time with warm water because more of the simple starches (glucose or short polymer chains) remained over the cloth later in the digestion step. Less material from the first few samples remained over the cloth, but more material remained over the cloth in later samples. Also, the extra material from later samples were whiter in appearance than the material from the earlier samples. This extra material could be passed through after stopping the suction, adding 50 mL of water at 80°C, stirring, and applying suction. The hot water rinse quickly produced samples that were brown to tan in color and had the thickness of the earlier samples. The filtering system that successfully worked to quickly filter the sample is shown in Figure 2.11.

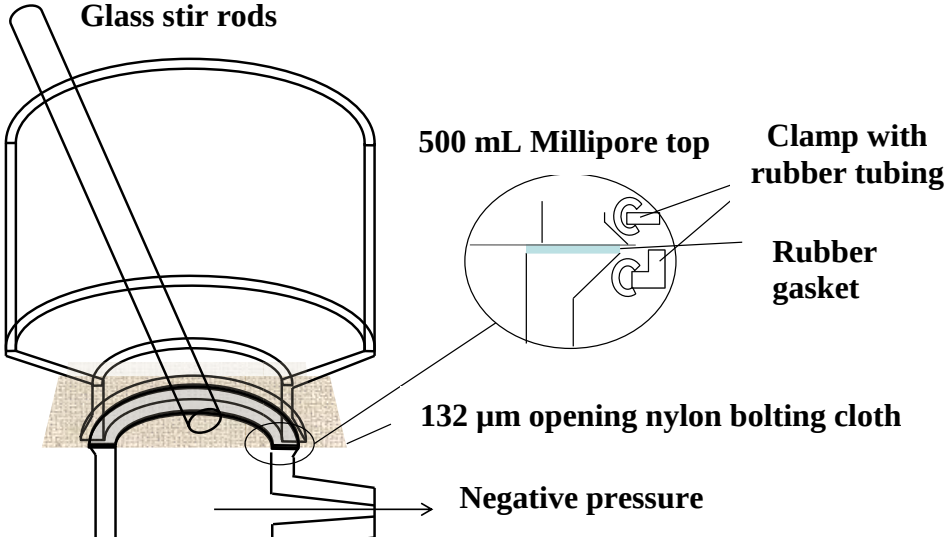

Figure 2.11 - Fourth filtering attempt scheme

The above filtering apparatus was selected because it was the quickest filtration system. The glass stirring rod was used during filtration to prevent the solid portion from clogging the openings of the sieve.

2.3 - Specimen preparation for imaging

The diameter of the sample left on the nylon cloth was too large for imaging and the nylon used for filtering is not on a NIR non-absorbing background. To get a sample that could be imaged, the filtered material needed to be removed from the nylon cloth, and to be collected on a smaller area matching the imaging field. A stainless steel disc with 80 µm openings was employed to separate the solid from the small amount of liquid involved in this specimen transfer.

2.3.1 - Recovering solid specimen from the nylon cloth

The sample was transferred into a 100 mL beaker with water and methanol. A metal spatula was used to remove the bulk of the solid specimen from the cloth. Only the protein that was tightly bound to the cloth remained. Submerging the cloth in an ultrasonic bath with 10 mL of water, ethanol, or 1: 1 (v: v) mixture left only a small residue of protein on the cloth. Using a microscope, no insect fragments were found to be present in the residue. The loss was presumed to be minuscule, reproducible and having negligible effect on the final results. The removed solid specimen was ready to be deposited onto a surface for imaging.

2.3.2 - Depositing solid specimen on imaging plate

A 10.28 mm (0.4 inches) diameter stainless steel filtering disc matched the instrument FOV (10.28 by 12.84 mm) imposed by the reflection collecting lens resulting in 40 micrometer pixels. Suction devices (filter beds) were made with stainless steel filter discs (80 µm openings) and sintered glass (70-100 µm openings) to locate the sample with this area dimensions. Unfortunately, the sample again took more than an hour to filter using aspiration and the steel filter disc or sintered glass, because of the increased thickness of the sample.

The first filtering device was made with the following items: a 3.5-inch tall plastic funnel 3 inches in diameter at the large end and 0.5 inches in diameter at the small end. The funnel tapered down to the smaller diameter over 2.5 inches with the spout adding another inch. At the spout of the funnel a serum cap was added (Precision Seal® Rubber Septa catalogue number Z554073, Sigma-Aldrich, St. Louis, MO): such caps are commonly used to seal a 14/20 standard tapper glass joint. The serum cap was 9/16 inch in inner diameter at the top and fit snuggly over the funnel spout. A 5/32 hole was bored into the center of the rubber serum cap. A sintered glass filter disc 7/16 inch in diameter and 1/8-inch-thick with 70-100 µm pores part number 7176-33, Ace Glass, Vineland, NJ) with an O-ring (part number SC0575, Brass Craft, Novi, MI) that had a 7/16-inch inner diameter and a 5/8-inch outer diameter and a 3/32-inch wall placed around it. This created a tight fit when the disc was placed inside the top end of the rubber serum cap. The spout of the plastic funnel was placed inside the larger end of the serum cap. The bottom end of the serum cap had a brass tube with a 3/16-inch outer diameter inserted for a tight seal. The bottom of the brass pipe was placed in a number 8 rubber stopper and inserted on the same flask used for the initial filtration. The cross-sectional view is shown in Figure 2.12.

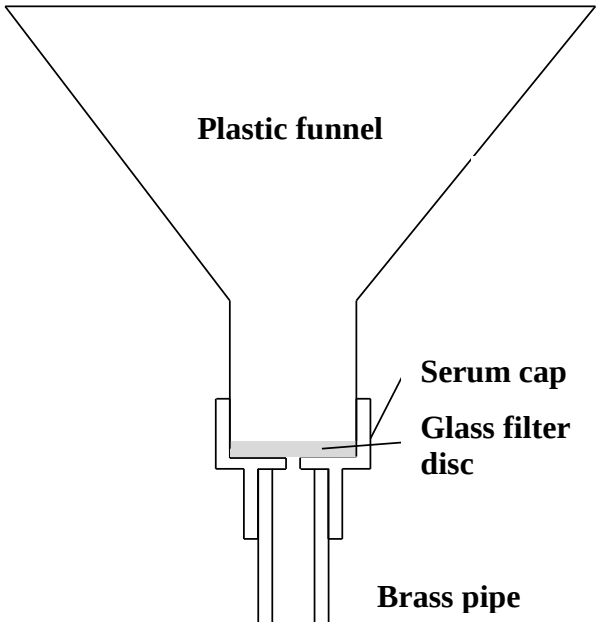

Figure 2.12 - First attempt at filtering sample onto an imaging surface

This filter apparatus was used to provide a high level of suction for the small area of a NIR non-absorbing surface. Even though less liquid had to be filtered and some of the sticky

protein and starch had been removed, the reduced surface area resulted in a thick filter cake. The deposited sample cake slowed the filtering process.

A small rubber washer was inserted to utilize the whole surface area for suction. The rubber washer was fabricated using cork borers to cut through 1/16-inch-thick sheet of rubber. The concentric holes of 3/8 inch and 7/16 inch resulted in the formation of the washer that added space between the sintered glass filter disc and the bottom of the rubber serum cap. This modification (Figure 2.13) did not increase the suction sufficiently to allow liquid to readily flow through the filter cake.

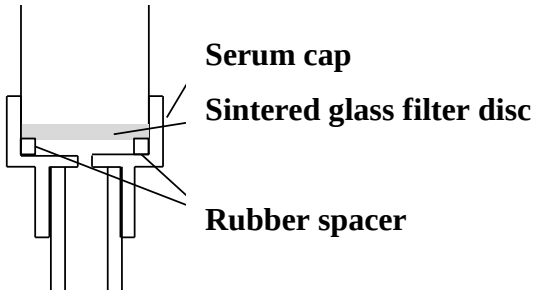

Figure 2.13 - Second attempt at filtering onto an imaging surface

This system was very similar to that of the first attempt (Figure 2.12), but a wider area of open suction filtration surface was achieved with a donut shaped rubber gasket.

The next attempt was to apply pressure over the liquid slurry instead of using suction done with all previous attempts. To do this, syringes were modified. A 5 mL BD Luer-Lok TM syringe with a luer lock tip (product number 301027, Franklin Lakes, NJ) was initially used. The syringe barrel was shortened to about 1.5 inches from the tip of the syringe barrel to enable removal of the sample disc. A perforated stainless steel disc 7/16 inch in diameter with 80 µm openings that fit snuggly into a syringe barrel was inserted into the syringe barrel covering the tip. The sample was poured in the syringe barrel and the plunger was inserted and pressed down to force the liquid through the filter and into a beaker. Compaction of the sample restricted the

liquid above the filter cake from readily passing through. A 20 mL BD Luer-Lok TM (product number 301031, Franklin Lakes, NJ) syringe, with a luer lock tip, was also tried. In this case the diameter was increased to 11/16 inch, resulting in some of the sample being sacrificed to provide a larger filter area. This was done even though not all of the sample area would fit into the imaging FOV. The increase in surface area did not increase filtration speed.

A syringe assembly was designed to employ backflow intermittently in order to loosen sample particles from the pores of the filter. The pneumatic connection was completed by using a female luer to female luer adapter (Cole-Parmer Item number EW-45508-22, Vernon Hill, IL). Using this adapter allowed both Luer Lock tips of syringe barrels to be joined together. On the side opposite the 20 mL syringe barrel equipped with the stainless steel filter disc, a 5 mL syringe barrel collected liquid that came through the filter. After liquid stopped passing through the filter, a small amount of liquid was back flushed through the filter. This back and forth fluid motion apparently broke up the clog, allowing improved filtration. When the pressure was reapplied in the forward direction, the filtering surface quickly clogged as previously reported. Although the three attempts described above offered little improvement for the benefit of future experimenters three syringe modifications used are shown in Figure 2.14.

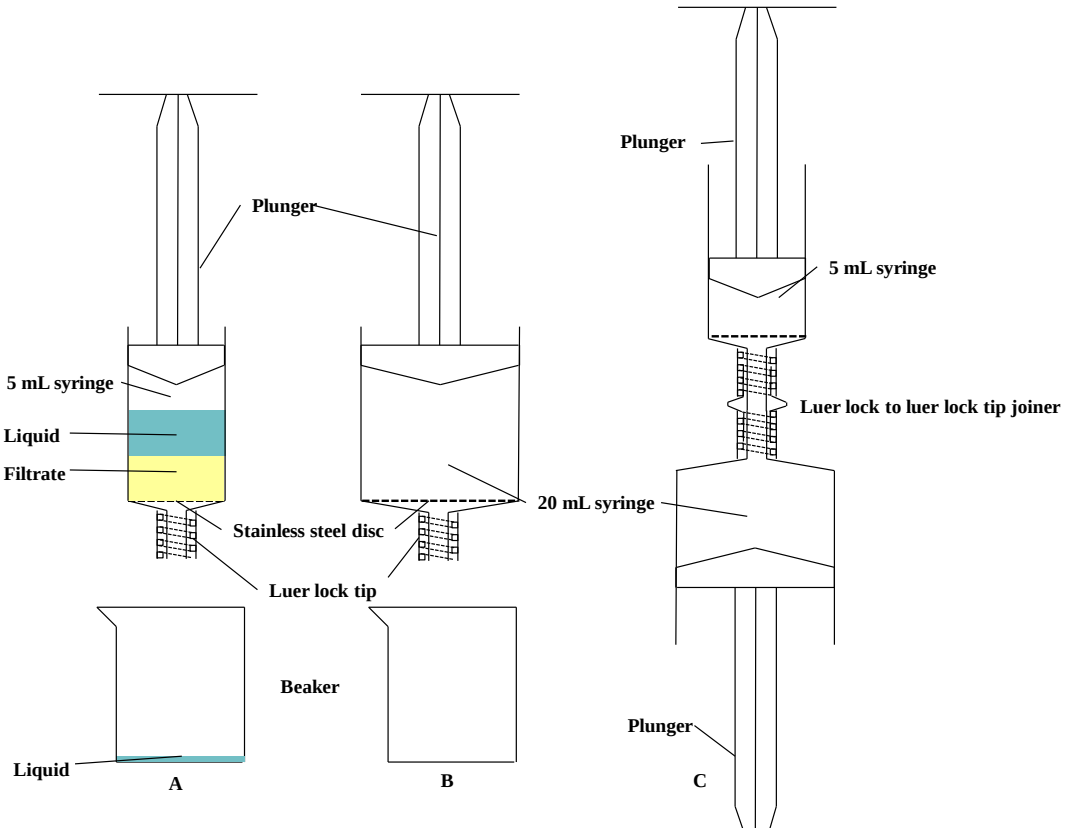

Figure 2.14 - Syringe attempts at filtering onto an imageable surface

The three attempts at using syringe barrels are shown above.

2.3.3 - Larger FOV used to increase filtering surface area

A larger, 25.4 mm diameter stainless steel filter disc (part number N29657B, McMaster-Carr, Elmhurst, IL) was used along with a modified suction apparatus to allow thinning the sample by having it spread out to a larger diameter. This greater specimen diameter required changing the lens on the instrument that produces an increased pixel size. The formerly 10.24 mm by 12.8 mm image dimension that had 40 µm pixels was replaced with a 120 µm pixel size allowing a 30.72 mm by 38.4 mm FOV to be imaged. The diameter of the sample cake could be up to 30.72 mm, so the 25.4 mm disc was small enough to avoid having any part of the sample outside of the FOV. Sintered glass at this dimension was rejected because it is not easily cleaned in comparison to a perforated stainless steel disc. Because the suction initially pulled the screen

into the suction flask several times, a back-wire support of thick steel mesh was placed under the disk to provide support.

Cutting holes in the base of a syringe barrel was initially attempted to provide support for the disc, but the pressure on the plastic syringe barrel caused it to lose its rigidity over time. After 5 to 10 uses with the syringe barrel base it no longer prevented the stainless steel disc from being pulled into the suction flask. The steel back support wire held up with continuous use. The O-ring was 7/8-inch inner diameter and 1-1/16-inch outer diameter with a 3/32-inch wall thickness (part number 580, Brass Craft, Novi, MI) made it difficult to remove the sample from the apparatus. Without the O-ring, however, the sample could leak around the seams and be lost with the filtrate. Using this method and the suction system shown in Figure 2.15, the liquid used to transfer the slurry into this suction system could be separated in less than 4 minutes. A 95% ethanol rinse of the sample replaced the residual water and the residual alcohol was readily vaporized. The valve was closed after ethanol was added. As the ethanol is sucked through the sample. it draws bound water out of the sample. A few minutes of air flow through the sample, dried the sample enough for spectroscopic analysis. Sample cakes ready for imaging were stored in a desiccator prior to analyses.

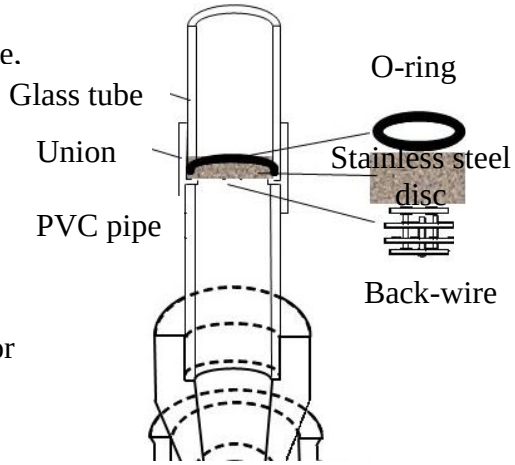

Figure 2.15 - Filtering apparatus for a solid sample to be imaged

This apparatus was chosen to quickly filter the sample through a stainless steel disc that does not absorb NIR and was small enough to fit the solid specimen in the medium FOV lens that provides adequate pixel resolution.

During overnight storage in the desiccator, edges of the samples curled upwards. To prevent the sample deformation, specimens were stored between two pieces of stainless steel screens, each of which were cemented to a Schedule 40 PVC pipe. The two pipes were slightly different in their dimensions. The larger pipe had a 2.385-inch outer diameter and a 2-inch inner diameter so, that the smaller pipe (inner diameter of 1.5 inch and outer diameter 1.90 inch) could slide into the larger pipe. The specimen to be imaged is placed on the steel screen from the larger diameter PVC pipe inside the pipe, the smaller PVC pipe was then placed inside of the larger pipe screen side down. This approach sandwiched the specimen in a breathable container without crushing or smearing it. The breathable containers were labeled and stored in a desiccator until the specimens were ready to be imaged. The step by step procedure is located in Appendix A on page 65.

Part 3 - Final method application

3.1 - Specimen preparation procedure

The sample preparation method that included the best procedure found in the development stage was used to concentrate and image bread quality wheat flour spiked with fragments of *Tribolium confusum*. The method began with particle size sieving to eliminate fine endosperm particles (less than 150 µm). The sample was further concentrated by hydrolysis of starch in the presence of fungal α-amylase to digest starch at an elevated temperature (80^0C). The elevated temperature caused starch gelatinization and increased enzymatic activity. The resulting small dextrins and other solubles were removed by wet sieving through nylon bolting cloth (132 µm opening). With elevated temperature driving the hydrolysis, this step provided results comparable to acid hydrolysis but without injurious fumes or corrosive damage to instrumental electronics.

The bolting cloth, combined with the use of a stirring bar to rub over the cloth allowed water and soluble components to pass through quickly yet prevented the protein and hemicellulose from clogging the openings of the bolting cloth. The bolting cloth had an NIR response which would cause a crisscross pattern in the image. An additional step eliminated the pattern and decreased the surface area of the sample for imaging. The solid residue was scrapped from the filtering cloth into a 50 mL beaker and the cloth was also rinsed with 95% ethanol. The rinse ethanol and residue were collected into the same 50 mL beaker. The solid residue in the 50 mL beaker is finally transferred to a filtering apparatus containing a 1-inch diameter stainless steel disc with 80 µm openings. The added ethanol causes precipitation of viscous polymeric components and facilitates filtration. The ethanol also dissolves bound water that is aspirated off from the solid sample by suction. If the sample is exposed to the stream of air for 5 minutes after

a rinse of alcohol it becomes dry enough to avoid interference when imaging. The solid residue can then be stored in a desiccator prior to imaging. The step by step procedure is in Appendix A on page 65.

3.2 - Experimental results

The first insect tested was the *Tribolium confusum* (confused flour beetle). The insect fragments were weighed into 50 grams of flour. The fragment spiked insects were concentrated and imaged. Results were calculated and with the exception of the highest and lowest concentrations, were linear and are represented in Table 3.1. The 0.092 ppt concentration level was below the level of quantitation and the 0.389 ppt concentration level was above the linear working range.

Insect added (ppt)	0.092	0.142	0.192	0.284	0.389
Image 1 % insect		6.74	4.69	7.11	9.71
Image 2 % insect	6.55	4.21	7.49	7.00	7.95
Image 3 % insect	3.75	3.77	6.11	8.08	6.46
Image 4 % insect	5.47	4.44	4.17	8.47	6.67
Mean % insect	5.26	4.79	5.62	7.67	7.7

Table 3.1 - Tribolium Confusum chemical imaging results in relative % insect area

Each of the five concentration levels were stated within +/- 0.006 ppt. The fragment concentration levels of the spiked specimens were by volume 0.092 ppt, 0.142 ppt, 0.192 ppt, 0.284, and 0.389 ppt. Each measurement of the added insect was the mean of four replicate specimens and was within +/- 0.006 ppt. The highest concentration level (0.389) was roughly two times the DAL, and the lowest value (0.092) was near to 0.5 of the DAL. The total range of insect fragment concentration was only 0.297 ppt in the dilute original specimens. The concentration levels for the specimens just below the DAL value and the specimens at the DAL

value itself were only 0.050 ppt prior to concentration. Despite the small difference in concentrations the calculated mean results got higher with increased concentration near the DAL.

Experimental results in general were lower when specimens appeared to contained more starch residue. This may have happened in the first filtering step if some specimens may have been stirred less aggressively during filtration or the undigested starch was not rinsed thoroughly after the liquid filtrate passed. Filter cakes were weighed to determine if there were noticeable differences in weight due to extra starch residue, but they were similar enough to not be concerned of an altered dilution factor. The high residual starch may have lowered the results by covering the insect fragment, because the starch was highly dispersive. The light would not be able to penetrate sufficiently to interact with the fragments.

(Figure 3.1-5) photographs of the specimens with the PLS score image next to each photograph (red indicates a location with a high concentration of insect and blue indicates an area of low insect concentration) for all 5 concentration levels of insect material was stated by volume. Results that were above the average for a concentration level of insect have a red box around them in Figure 3.1-5 and include specimens 38, 40, 41, and 46. Results that were below the average for a concentration level have a blue box around them and include specimens 43,48, 55, and 56.

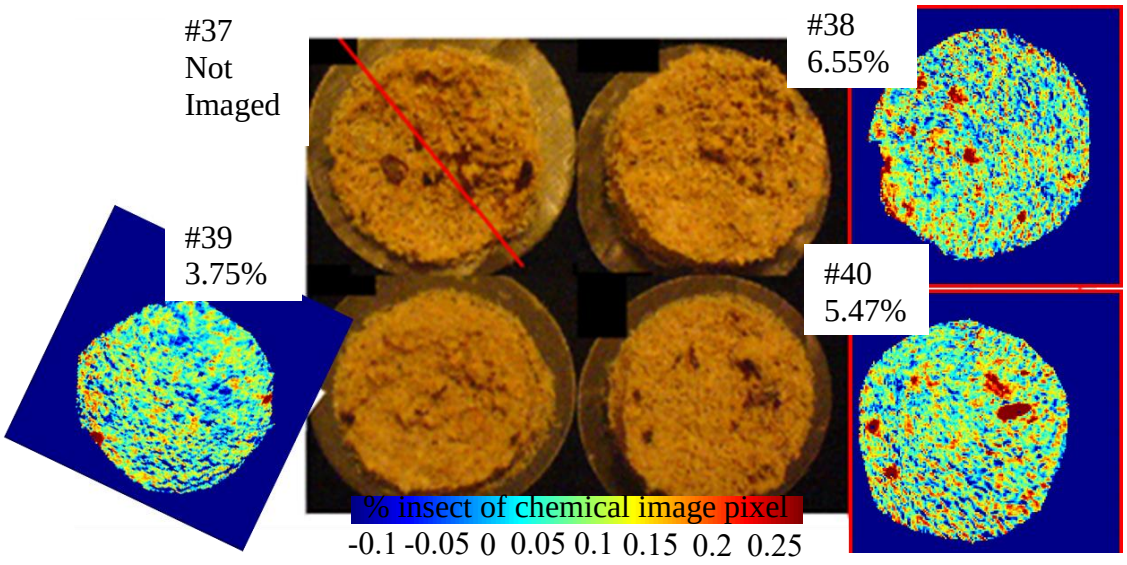

Figure 3.1 - 0.092 ppt of insect fragment level, photographs (center) chemical image outside (outside)

These specimens were from the lowest fragment concentration level. Specimen 37 was not imaged, because the screen broke and a noticeable amount of material was lost. Specimens 38 and 40 both raised the average. Both appeared to have numerous surface fragments. Note also voids on the top right corner of the section and that this was below the level of quantitation.

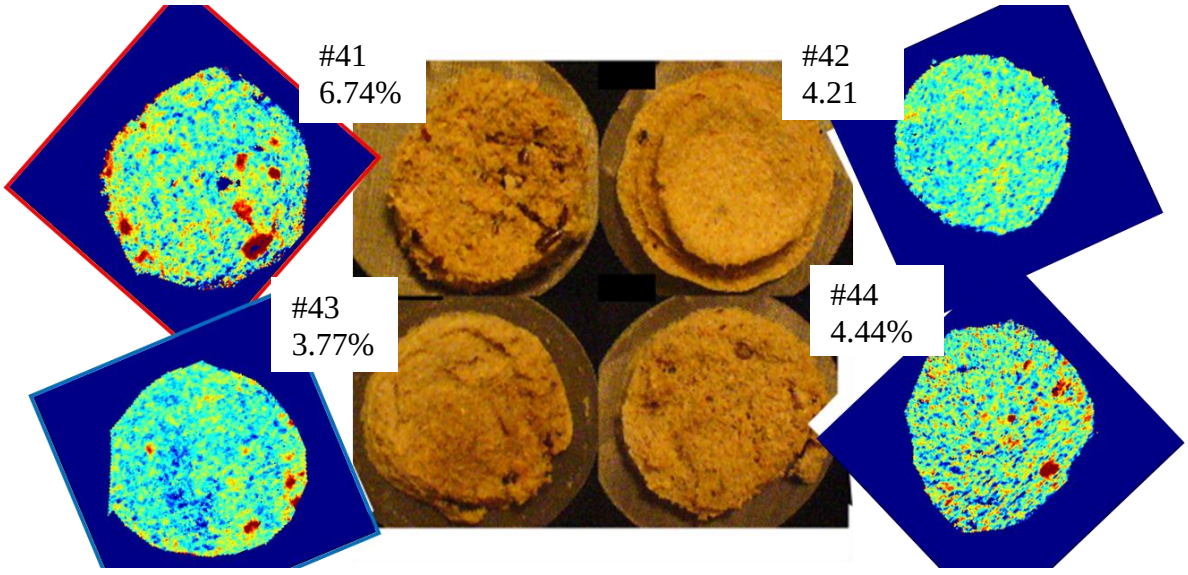

Figure 3.2 - 0.142 ppt of insect fragment level

This was the second level of fragment concentration. From the photo specimen 41 appeared to have more residual starch than normal and had a high calculated insect result. Specimen 43 had a low result, and the top left portion had a white starchy appearance in the photograph. Despite the odd shape 44, along with 42, was close to the average.

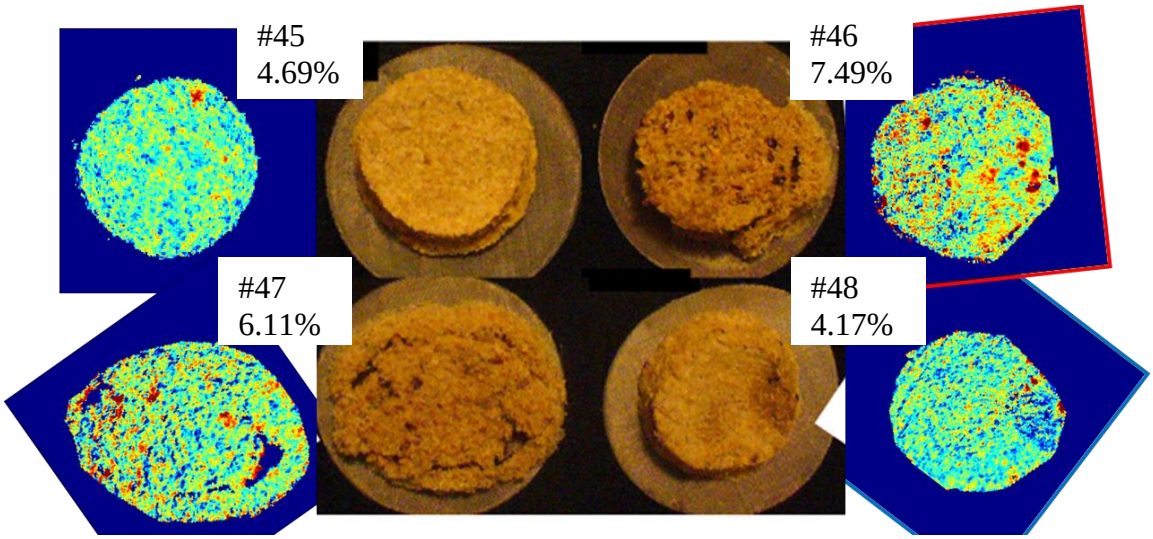

Figure 3.3 - 0.192 ppt of insect fragment level

These images were at the DAL for fragment concentration. Specimen 46 had a high result and appeared darker in color and has an odd shape. Specimens 45 and 48 had a low result and appeared to have a white color, indicating that undigested starch obscured most of the insect fragments.

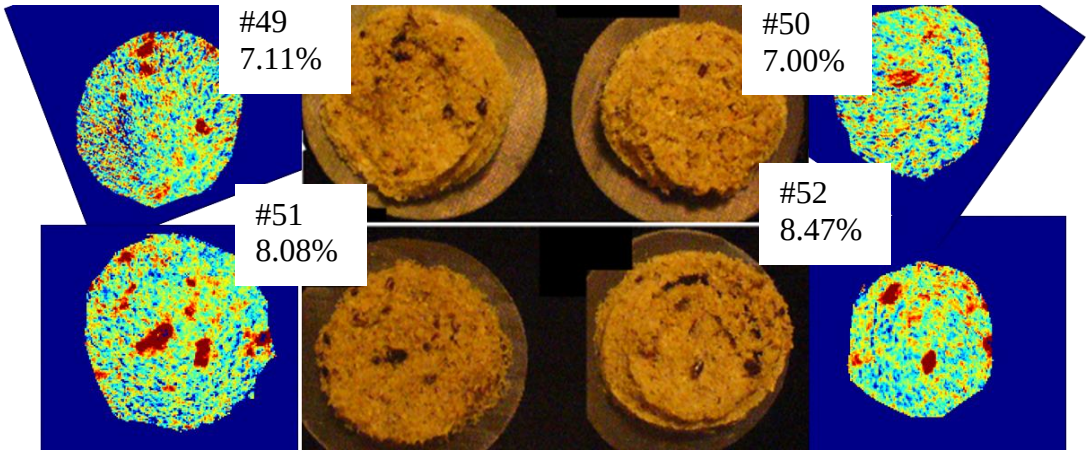

Figure 3.4 - 0.284 ppt of insect fragment level

These images were from the second highest concentration. All the values were clustered together. Image 50 appeared to have starch residual obscuring fragments.

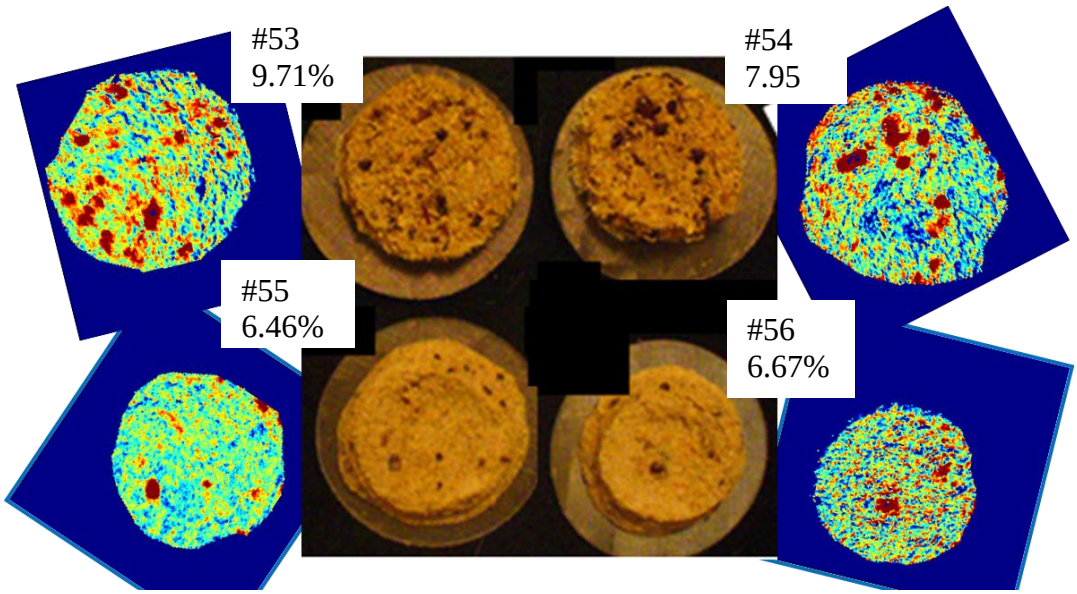

Figure 3.5 - 0.389 ppt of insect fragment level

These images were the highest fragment concentration. Specimens 55 and 56 had a white smooth texture indicting that more residual starch was present in these filter cakes.

Some images had very low calculated insect concentrations. Their photographs were smooth giving the appearance of a thin layer of starch that was not properly removed by the starch digestion process. Starch was a light scattering material that would prevent the incident

NIR radiation from penetrating below the specimen surface. *Tribolium confusum* specimens 42, 43, 45, 48, and 50 were probed after measurement for the presence of residual starch, with a starch-iodine test procedure. Specimens 55 and 56 also appeared to have a high starch content, but insect fragments were still seen on the top layer, so the obscuration effect was partially reduced.

The starch-iodide test was utilized by obtaining iodine solution (Lugol's) of 1.8% iodine and 3.0% potassium iodide. The solution created a tri-iodide that reacted with amylose producing the (I_3^-) species that has an intense dark blue or purple color. Small sections of specimens 43 and 46 were removed and tested with various dilutions of the Lugol's solution. The original solution concentration worked best to detect the suspected specimens with high residual starch (43) and the suspected low starch specimen (46).

Figure 3.6 - Starch test for specimens 43 and 46

The specimens had two drops of starch indicator solution dropped on them. On the left is a photo of sample 43, which has the lowest value of the 0.142 ppt value of insect fragments. The dark color indicated the presence of starch. The photo on the right was of specimen 46 which had the highest insect value for the 0.192 ppt value of insect fragments. The lack of dark color development indicated that any starch left in this specimen was below detection limit. It was also noticed that 43 become spongy and pliable, but 46 remained firm when it soaked up the

moisture. The pliability of the sample may be caused by the presence of starch throughout the sample.

Figure 3.7 - Starch test for specimen 42

Specimen 42 had starch indicator added to it because it was the second lowest value for the 0.142 ppt of insect fragments. Color developed indicating it also had a high residual starch. Yet it did not become spongy like specimen 43; the majority of the starch residue may have been on the surface.

Figure 3.8 - Starch test for specimen 45

Specimen 45 had starch indicator applied to it, since it had the second lowest value for the 0.192 ppt level. The dark purple color developed indicating high starch content. It also did not get spongy.

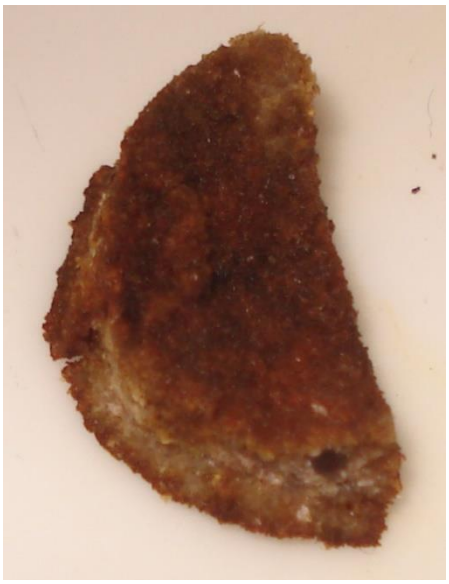

Figure 3.9 - Starch test for specimen 48

Specimen 48 had the lowest value of the 0.192 ppt level did not develop the dark color but became spongy. This specimen may have had starch below the surface.

Figure 3.10 - Starch test for specimen 50

Specimen 50 had the lowest value for 0.284 ppt and appeared to have a layer of starch. The dark color developed indicating the presence of starch.

Figure 3.11 - Starch test for specimen 55

Specimen 55 had the lowest value for the 0.389 ppt level also had dark color development.

Figure 3.12 - Starch test for specimen 52

Specimen 52 from the 0.284 level was tested for starch. It was a physically odd sample that had the smooth starchy look of some the specimens with a low calculated insect content. Yet it received the highest calculated insect concentration for its level of added insect. From this

photo and the chemical image, it is clear that the insect fragments were present on top of the starch.

Specimens 43 and 46 were tested together to determine if a starch residue layer caused lower calculated results. Specimen 43 was a filter cake with low values and 46 was one with a high value relative to other replicates of the same level of added insect. This was suspected to be due to one sample (43) having a layer of starch on the top and the other sample (46) not, leaving all the insect fragments exposed. The color difference in the two specimens supported this claim. Three more low specimens 42, 45, 50 also had a very dark color. Another low specimen 48 did not turn as dark as the other low samples. Although the layer of starch was not thick it did cover insect fragments and developed a spongy texture after addition of the Lugol's solution. In this case increased starch throughout the thicker filter cake obscured some of the fragments. Specimen 55 had a fragment concentration beyond the linear measurement, had a low value, and tested positive for starch. At this level there were still visible insect content on the surface, but sufficient fragments were obscured to cause a low calculated insect concentration. The experimental hazard of measuring high starch filter cakes was obscuration of fragments by scattering of the light before it interacts with insect fragments. From specimen 48 it was obvious that the sample thickness covered and thus obscured the insect even though it did not test positive for a high starch residual on its surface. From specimen 52, a high starch filter cake with a high insect count, it was noted that the fragments may fall on the top of a starch layer, but it is more likely the fragments will be obscured. (Figure 3.13) plotted the middle three insect concentrations excluding images 42, 43, 45, 48, and 50 to include data that was not altered due to a high amount of starch obscuring the fragments.

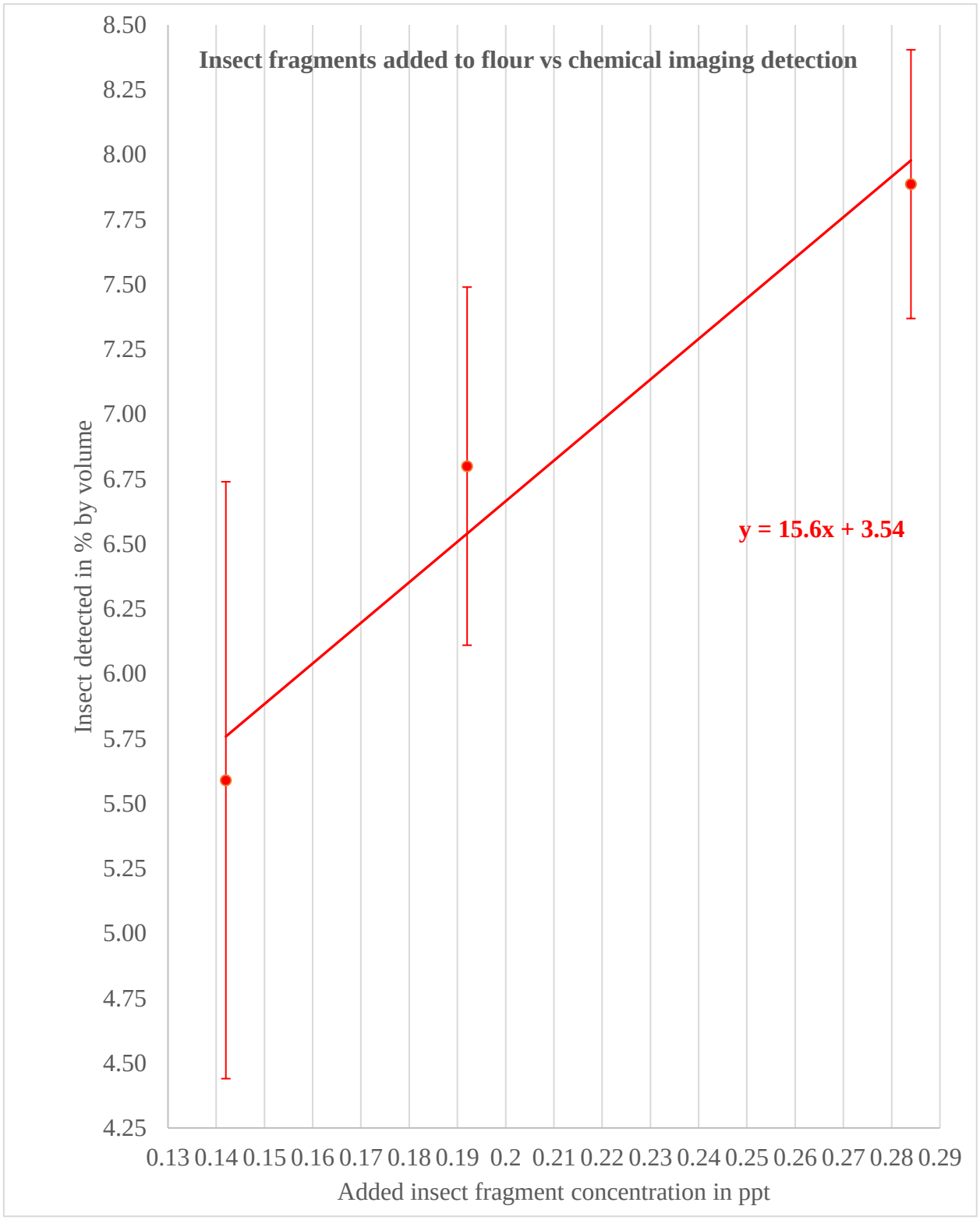

Figure 3.13 - Tribolium confusum linear means and average deviation from mean

The plotted mean of the images that were not removed due to starch residual are shown with red dots. The error bars were the average deviation from the plotted mean. The red line was a best fit plot. The equation for the linear relationship was displayed in red.

The second insect tested, *Sitophilus oryzae* (rice weevil) had specimens with concentration levels of insect by weight of 0.095 ppt, 0.142 ppt, 0.195 ppt, 0.251 ppt, and 0.285 ppt. The results at each of these levels are shown in Table 3.2. The highest two concentrations (0.251 an 0.285 ppt) were placed closer to the DAL, because on the first insect indicated a flattening of the slope after 0.285 ppt.

Insect added (ppt)	0.095	0.142	0.195	0.251	0.284
Image 1 % insect	0.6	6.71	6.59	8.23	
Image 2 % insect	3.64	5.19	5.23	6.4	6.02
Image 3 % insect	3.75	2.34	5.32	5.97	6.73
Image 4 % insect	5.84	1.22	6.6	7.43	7.88
Mean % insect	3.46	3.87	5.94	7.01	6.88

Table 3.2 - Sitophilus oryzae chemical imaging results in relative % insect area

Included in Table 2 are all the individual image values at each concentration levels and the mean value of each image. Each of the five levels were within +/1 0.006 ppt. In Figure 3.10 A-E individual chemical images with photographs are analyzed, and specimens with the appearance of high residual starch are tested with Lugol's solution as previously described. The largest obscuration of fragments appeared to be from 0.142 ppt concentration level, but the other two concentration levels in the linear range had specimens that had the appearance of a residual starch layer on the top.

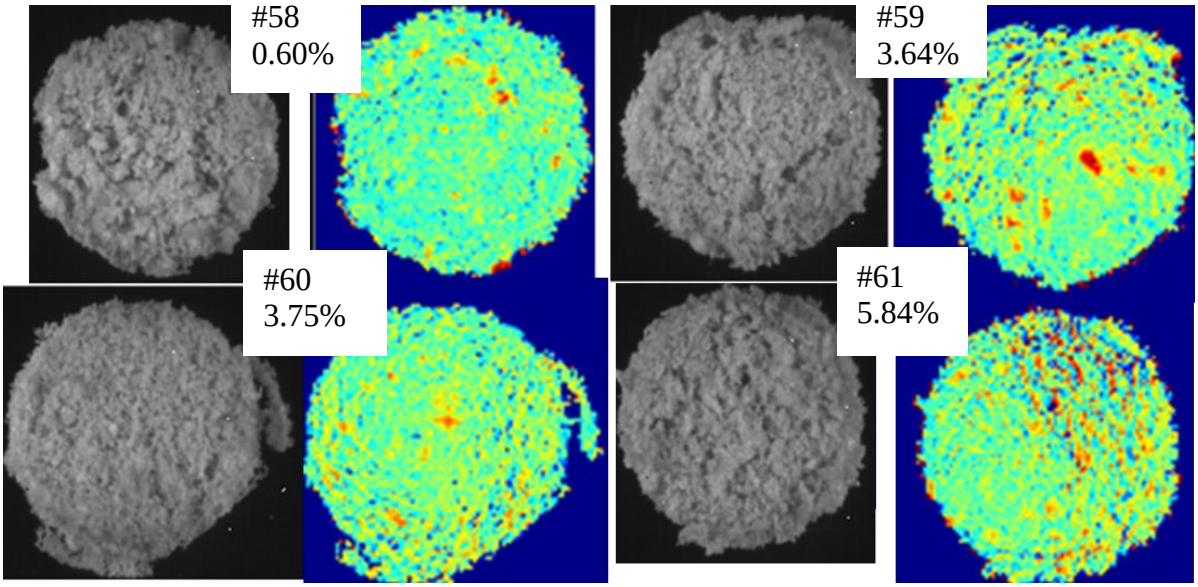

Figure 3.14 - 0.095 ppt insect concentration level, black border instrument image photograph and blue border chemical image of insect fragments

These images were from the lowest concentration level. The mean of the four images appeared in line with the slope, but the average deviation was large. The deviation was large because digested starch residue on specimen 58 covered the insects and specimen 61 had a high result due to collecting a non-representative subsample of the heterogenous material.

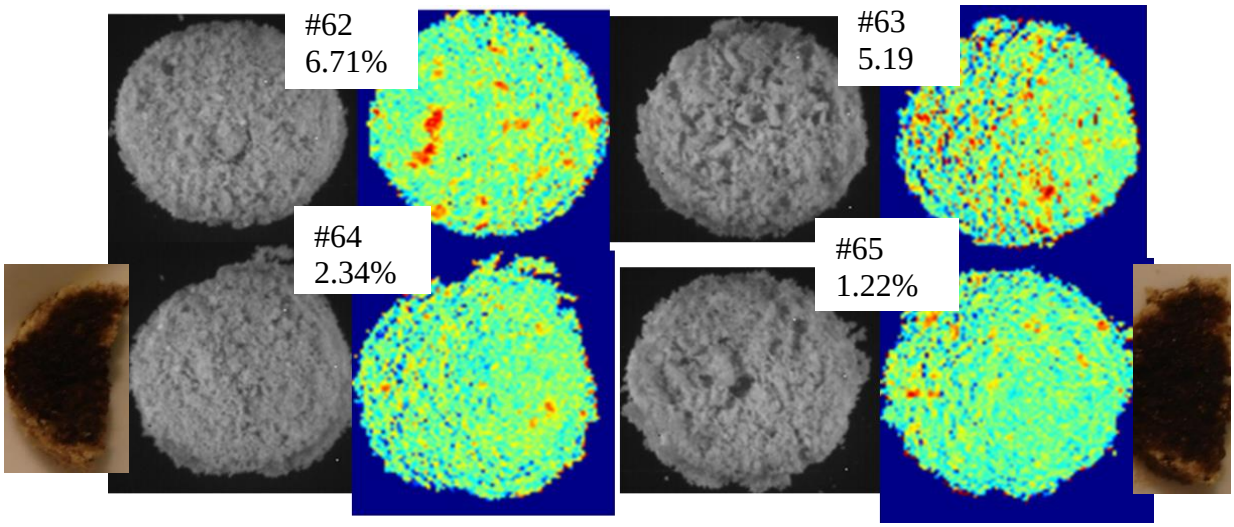

Figure 3.15 - 0.142 ppt insect concentration level, outer photos of starch test

These were the figures from the second lowest insect concentration level. This level also had a high average deviation. Specimens 64 and 65 appeared to have very few fragments on the surface while numerous fragments were on the surface of specimen 62. Result of a positive starch test is included for specimens 64 and 65.

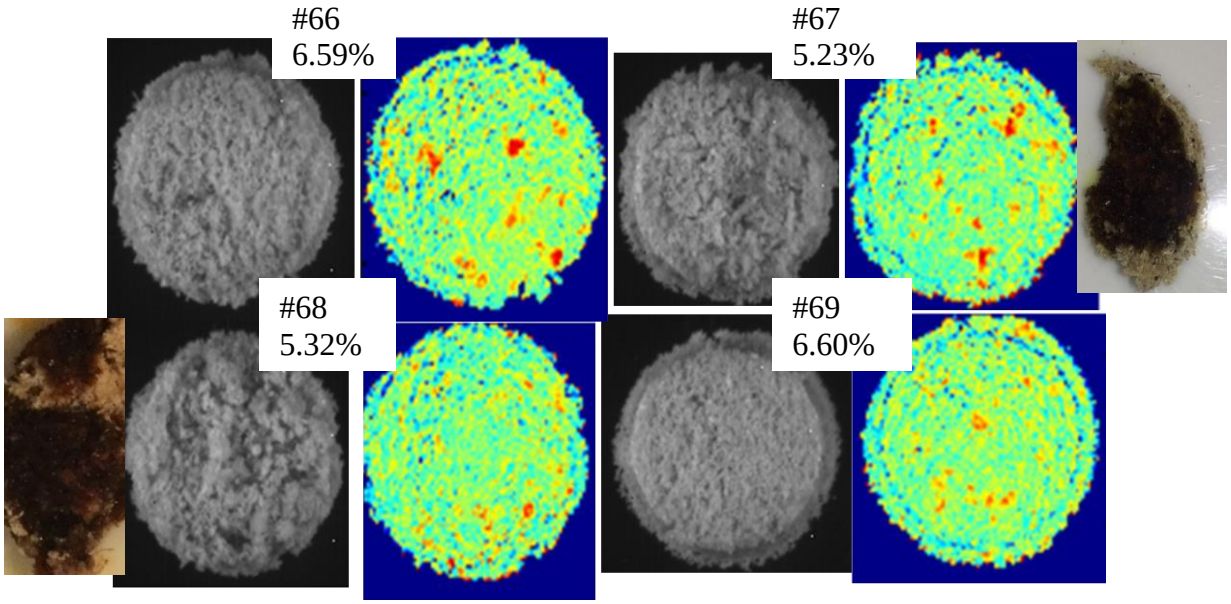

Figure 3.16 - 0.195 ppt insect level

This was the level at the DAL. The average deviation was low, but specimens 67 and 68 clustered near the same level below the other two specimens and had a white rough surface. The two photos on the outer edge were of the positive starch test for specimens 67 and 68.

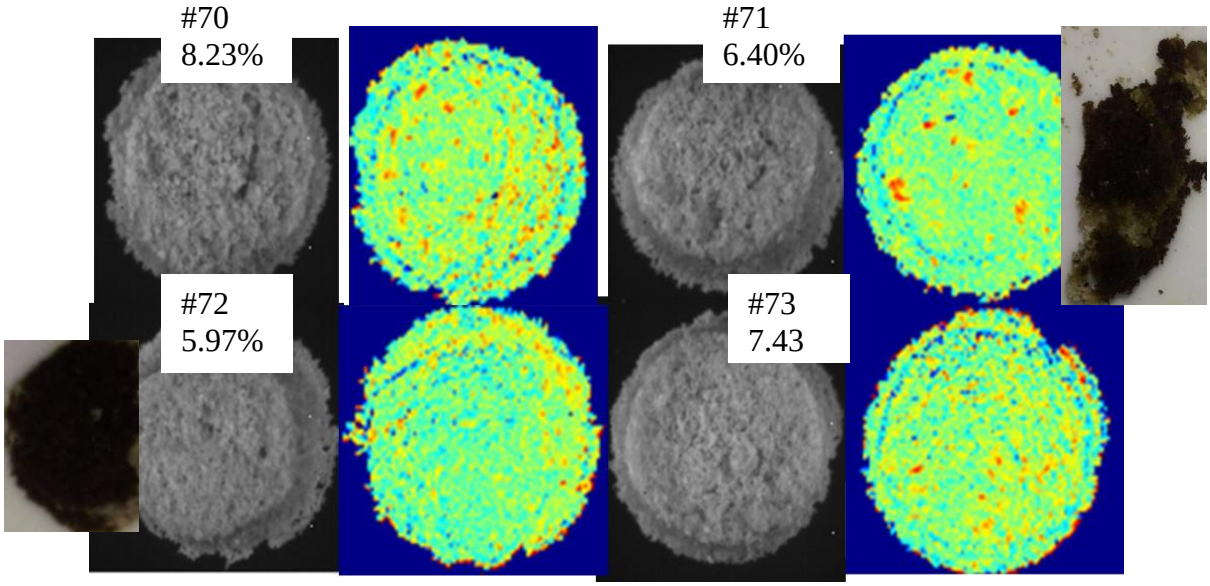

Figure 3.17 - 0.251 ppt insect level

These images were from the second highest concentration level. The average deviation was small. Specimen 72 was a very thick specimen that was suspected to have a high amount of starch. Specimen 71 also looked thick, both of these filter cakes were tested for starch, shown on the outer edge of Figure 3.17. The dark color developed indicating a high starch residual.

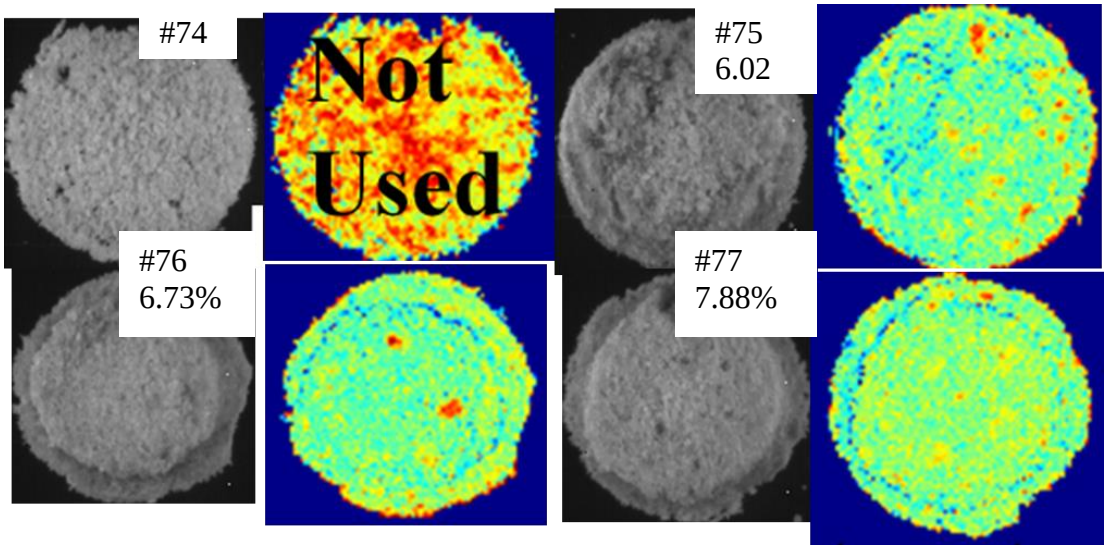

Figure 3.18 - 0.284 ppt insect level

These images were from the highest concentration level. Specimen 74 was partially lost when the stainless steel screen was pulled into the suction flask. The image was not calculated

for insect fragments. The other three images were somewhat low and appeared to not have very many fragments on the surface.

Although not that drastic with the exception of specimens 64 and 65, the images that were skewed low and tested positive were excluded from the plot of the *Sitophilus oryzae* insect concentration level vs chemical detection in Figure 3.19. The first insect is plotted alongside it for comparison. Since the slopes and offsets of the plots are comparable, determination of insect concentration may be done without knowledge of the insect species or if there are multiple insect species present.

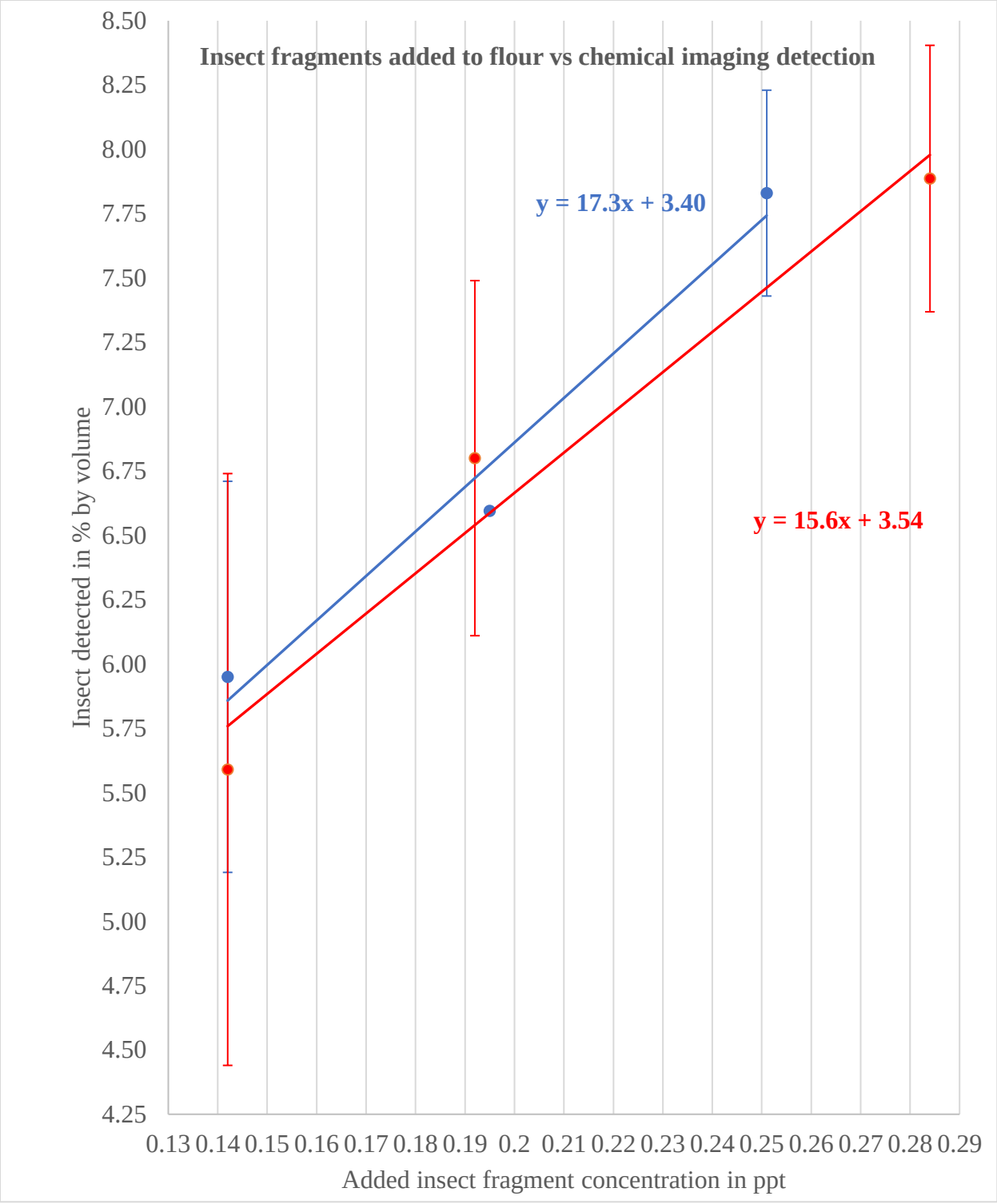

Figure 3.19 - Sitophilus oryzae plot of linear range with the Tribolium confusum plot superimposed from Figure 3.13

The plot of added insect fragment versus insect detected for *Sitophilus oryzae* is shown in blue and for comparison *Tribolium confusum* is shown in red. Error bars indicated the average deviation of insect detected from the mean. The equation for the linear relationship for each insect are shown in their respective color.

The two insect plots after irregular specimen data results were removed had very similar slopes; 15.6 for *Tribolium confusum* and 17.3 for *Sitophilus oryzae.* The *Tribolium confusum* is only approximately 0.30 % under the *Sitophilus oryzae* value of detection at the high end of the linear working range. At the low concentration end of the linear working range the offset is approximately 0.15% between the two insects. The similar response in detection indicated that this method could be used without knowledge of insect species or if multiple species had contributed to the amount of insect fragments in a flour source.

3.3 - Conclusion

Determining the extent of extraneous material in the form of insect fragments in high quality bread flour was a difficult task, because the legal defect action limit (DAL) is set at a low concentration of insect fragments. Utilizing the benefits of NIR imaging to aid in this task was seriously explored as an alternative to the unreliable fragment count. Unfortunately, a concentration step before imaging was necessary and was ultimately incorporated because of the low DAL. After many attempts, a working concentration method was obtained. The method utilized physical concentration by removing finely granulated endosperm, followed by an enzymatic concentration step using α-amylase digestion of starch at elevated temperatures. To maximize the time spent on sample concentration a batch process was developed that could prepare many samples at the same time for subsequent imaging.

The concentration method developed was tested by spiking bread baking quality wheat flour with *Tribolium confusum* and *Sitophilus oryzae* fragments at several concentrations. Concentrated specimens were spectroscopically imaged by NIR at the designated wavelength range to generate a linear response to the added insect fragments of known concentration. Insect fragments were chemically distinguished due to the high protein content of the insects and the presence of chitin which had a defined peak at 2050 nm. The calculated concentration of insect increased with addition of insect fragments calculated from the mean of replicate FOVs that did not have obscuration of fragments by residual starch. Five regulatory-applicable concentration levels 0.092 ppt, 0.142 ppt, 0.192 ppt, 0.284 ppt and 0.389 ppt +/- 0.006 ppt for the *Tribolium confusum* were chemically imaged. The *Sitophilus oryzae* added concentration levels were 0.095 ppt, 0.143 ppt, 0.195 ppt, 0.251 ppt, and 0.285 ppt +/- 0.006 ppt. For each insect the middle three

concentration levels were plotted, because the highest level was above the limit of linearity and lowest value was below the limit of quantitation for both insects.

The chemical distinctions detected by the imaging equipment, enabled linearity over a regulatory applicable range even with randomness in fragment placement, after low values were removed. Furthermore, the plots had a very similar slope and a small offset, so that a limit of rejection based of the test could be performed regardless of the species of insect fragments present or if there are multiple types of insects.

Future work may include an approach that could hasten the concentration and preparation method or allow for better chemical distinction could be to apply the sample onto a wider, stainless steel disc for imaging. The increased surface area would result in a thinner sample cake to decrease the chances of an insect fragments being buried in the sample. Other enzymes such as hemicellulase (xylanase) or protease with dithiothreitol could be used in tandem with the α-amylase to digest more of the flour components. The sample could be centrifuged to separate the liquid from digestate. The floatation method could be explored instead of digestion to concentrate the sample onto a surface for imaging. There may be ways to improve the concentration method but, NIR chemical imaging can be used to determine the amount of insect material in flour. The fragment count does not define the quantity, because fragments may be small or large depending on sample handling. Chemically imaging of heterogenous mixtures like insect fragments in flour, may have some random variation due to where the fragments happen to land in the filter cake, but results are calculated with numerically distinct values. The ability to quickly image multiple images minimizes the effect if random fragment placement to strengthen the confidence in the detected value.

References

AACC International Method 28-03.02 Special Techniques for Extraneous Matter Methods. http://dx.doi.org/10.1094/AACCIntMethod-28-03.02

AACC International Method 28-41.03 Acid Hydrolysis Method for Extracting Insect Fragments and Rodent Hairs---Light Filth in white Flour http://dx.doi.org/10.1094/AACCIntMethod-28-41.03

Brader B, Rachel C, Plarre R, Burkholder W, Kitto G, Polston L, Dorneanu E, Szabo I, Mead B, Rouse B, Sullins D, Denning R. 2002. A comparison of screening methods for insect contamination in wheat. J Stored Prod. Res. 38 (1): 75-86.

Bonwell E, Fisher T, Fritz A, Wetzel D. 2008. Determination of endosperm protein secondary structure in hard wheat breeding lines using synchrotron infrared microspectroscopy. Vib. Spectrosc. 48 (1): 76-81.

Dogan H, Subramanyam B. 2017. Analysis for Extraneous Matter. Nielson S. (ed.). Food Analysis. Fifth Edition. Springer International Publishing. Ch 34: 599-614. DOI 10.1007/978-3-319-45776-5_34.

Dogan H, Smail V, Wetzel D. 2008. Discrimination of isogenic wheat by InSb focal plane array chemical imaging. Vib. Spectrosc. 48 (2): 189-195.

Fulcher G. 1982. Fluorescence microscopy of cereals. Food Microstruct. 1 (2) Article 7: 167-175. https://pdfs.semanticscholar.org/ecc4/12cc2762c203f1a6cfe51071367dbbe1d68b.pdf

Hyde A, Zultanski S, Waldman J, Zhong Y, Shelvin M, Peng F. 2017. General Principles and Strategies for Salting-Out Informed by the Hofmeister Series. Org. Process Res. Dev. 21: 1355-1370. DOI 10.1021/acs.oprd.7b00197. https://pubs.acs.org/doi/pdf/10.1021/acs.oprd.7b00197

Johnson M. 2016. Detergents: Triton X-100, Tween-20, and More. Materials and Methods. DOI //dx.doi.org/10.13070/mm.en.3.163. https://www.labome.com/method/Detergents-Triton-X-100-Tween-20-and-More.html

Koc H, Wetzel D. 2007. Imaging Local Chemical Microstructure of Germinated Wheat with Synchrotron Infrared Microspectroscopy. Spectroscopy. 22 (10): 24-32.

Lewis N, Kidder L, Lee E. 2005. NIR Imaging—near infrared spectroscopy on steroids. NIR News. 2 (6): 3-4.

Lewis N, Treado P, Reeder R, Story G, Dowrey A, Marcott C, Levin I. 1995. Fourier Transform spectroscopic imaging using an infrared focal plane array detector. Anal. Chem. 67 (19): 3377-3381.

Lyon R, Lester D, Lewis N, Lee E, Yul L, Jefferson E, Hussain A. 2002. Near-Infrared Spectral Imaging for Quality Assurance of Pharmaceutical Products: Analysis of Tablets to Assess Powder Blend Homogeneity. AAPS ParmSciTech. 3 (3) article 17.

Perez-Mendoza J, Throne J, Maghirang E, Dowell F, Baker J. 2005. Insect Fragments in Flour: Relationship to Lesser Grain Borer (Coleoptera: Bostrichidae) Infestation Level in Wheat and Rapid Detection Using Near-Infrared Spectroscopy. J Econ. Entomol. 98 (6): 2282-2291.

Perten Instruments. 2015. The Gluten Index Method. http://www.perten.com/Products/Glutomatic/The-Gluten-Index-method/

Perten Instruments. Glutomatic System Operation Manual. http://www.granotec.com.br/arquivos/Sistema_Glutomatic.pdf

Pussayanawin V, Wetzel D, Fulcher G. 1988. Fluorescence detection and measurement of ferulic acid in wheat milling fractions by microscopy and HPLC. J. Agric. Food Chem. 36 (3): 515–520. DOI: 10.1021/jf00081a027.

Ridgway C, Chambers J. 1996. Detection of External and Internal Insect Infestation in Wheat by Near-Infrared Reflectance Spectroscopy. J Sci Food Agric. 1: 251-264.

Sec. 137.105 Flour, Title 21—Food and Drugs, Volume 2 Chapter 1—Food and Drug Administration Department of Health and Human Services, Subchapter B—Food for Human Consumption Revised April 1, 2015.

Smail V, Fritz A, Wetzel D. 2006. Chemical imaging of intact seeds with NIR focal plan array assists plant breeding. Vib. Spectrosc. 42 (2): 215-221.

Sweat J. 1996. Variations in Tempering Times for Winter Wheats by IR Microspectroscopic Tracking of D_2O. Master's thesis. Kansas State University, Manhattan, KS.

Wetzel D, Boatwright M, Brewer L. 2010. Granular solid formation commodity mixture uniformity revealed via InSb focal plane array chemical imaging. Vib. Spectrosc. 53 (1): 83-87.

Wetzel D, Posner E, Dogan, H. 2010. InSb Focal Plane Array Chemical Imaging Enables Assessment of Unit Process Efficiency for Milling Operation. Appl. Spectrosc. 64 (12): 1320-1324.

Wetzel D, 2013. Positive Assessment of Mill Stream Endosperm Purity Using Chemical Imaging. Cereal Foods World. 58 (3):133-137.

Appendix A - NIR imaging stepwise specimen preparation procedure

I. Preparing samples for NIR imaging
   a. Physical Concentration
      i. Equipment
         1. Ro-Tap Sieve
         2. 150 µm opening Tyler Sieve
         3. Flour Pan
         4. Analytical Balance
         5. Camel hair brush
         6. Weighing pan with pouring spout
         7. Sealable jar to hold concentrated sample
      ii. Material
         1. Samples of appropriate 100 g size
      iii. Sequence
         1. Tare the flour pan.
         2. Assemble the Ro-Tap with only the 150 µm and the flour for sieving.
         3. Place the 100 g sample in the 150 µm sieve. Secure the Ro-Tap lid over the sieve and lower the Ro-Tap lever on the lid.
         4. Set the timer to 1 minute 30 seconds and turn on the Ro-Tap.
         5. Obtain the tare weight of the weighing pan.
         6. Transfer the sieve overs to the pan and weigh the overs and the weighing pan.
         7. Sieve overs = Weighing pan and overs – Pan tare weight
         8. Weigh the flour pan with the sieve thrus.
         9. Sieve thrus = Flour pan and thrus – Flour pan tare weight
         10. Store the overs in tightly sealed jar. The thrus may be retained.
         11. Use the overs to proceed to α-amylase digestion.
         12. Sieve remaining samples in similar fashion.
   b. α-amylase digestion
      i. Equipment
         1. Water bath to maintain a temperature 80^0C
         2. Hot plate to boil water
         3. Beaker to hold boiling water over hot plate
         4. Test tubes (50 x 305 mm)
         5. Glass stirring rods
         6. Thermometer for water bath
         7. 2 test tube racks (1 in the water bath, 1 one lab bench)
         8. Pipette (volumetric bulb to 0.2 mL volume capacity)
         9. 100 mL graduated cylinder
      ii. Material
         1. Distilled water for α-amylase digestion
         2. Concentrated α-amylase solution
         3. Tap water to fill the thermostated water bath and beaker for boiling
      iii. Sequence
         1. Heat the water bath containing a test tube rack to 80^0C.

2. Label test tubes by number.
3. Add 40 mL of distilled water to each test tubes.
4. Place flour samples in test tubes.
5. Pipette 0.2 mL of the α-amylase solution and add 30 mL of distilled water to each tube. Stir each mixture with a stirring rod.
6. Submerge test tubes in heated water using the test tube rack to keep tubes upright.
7. Samples are heated to 80^0C in 15 minutes and held there for 60 minutes.
8. After 75 minutes of digestion, transfer tubes to the boiling water for 5 minutes.
9. Remove tubes from boiling water and allow them to cool at room temperature.
10. Once all the samples have been digested and the enzyme denatured by heat, continue to the filtering procedure.

c. Filtering digested samples
   i. Equipment
      1. Suction set up 1 (large surface area to filter starchy slurry)
         a. 132 µm opening nylon cloth squares 2.5 by 2.5 inches
         b. 300 mL Millipore liquid sample holder
         c. 1-liter suction flask
         d. Rubber ring seal between the suction flask and Millipore holder
         e. Clamp that secures the Millipore filter assembly
      2. Suction set up 2 for drying samples into a cake for imaging analysis
         a. 80 µm opening stainless steel wire cloth
         b. Gooch crucible holder
         c. Glass sample holder that fits into form molded 1-inch PVC pipe holder
         d. Back wire support
         e. Rubber stopper with a hole that fits around a 1-inch PVC pipe
      3. Trap
         a. Large suction flask
         b. Two pieces of thick wall tubing
         c. Water aspirator
      4. 50 mL glass beaker
      5. Stirring rods
   ii. Material
      1. Distilled water
      2. 95% Ethanol
   iii. Sequence
      1. After allowing the digested samples to cool, add 50 mL of distilled water to the digested samples before transferring the sample to the first filtering system.
      2. The slurry is stirred with a glass rod, while gently rubbing the rod against the nylon filtering cloth. (Be sure the rod does not have sharp edges)
      3. Add 50 mL of distilled water to the empty test tube and stir it around and pour it to the Millipore funnel top to make sure all the insect fragments are out of the test tube and into the filtrate.
      4. Remove the sample from the nylon cloth by scrapping with a metal spatula into a 50 mL glass beaker and then rinse the filtering cloth.
      5. Use a glass rod to transfer the sample into the second filtering system.

6. Rinse the beaker and sides of the glass top of the suction system.
7. Once the liquid has been filtered, rinse the residue with 5 mL of 95% ethanol.
8. Draw air through the filter cake.
9. If images will not be collected right away, store the final sample cake in a desiccator until it can be analyzed with NIR imaging. Take precautions to not mix samples are crush them during storage.